SUBUNIT PEPTIDE-ENCAPSULATING NANOPARTICLE HIV VACCINE TARGETING CYTOTOXIC T LYMPHOCYTE ACTIVATION VIA PROTAC-ENHANCED CROSS PRESENTATION

by

Victoria Grace Trantow

A thesis submitted to Johns Hopkins University in conformity with the requirements for the degree of Master of Science in Engineering

Baltimore, Maryland

December 2022

Abstract

Development of an effective prophylactic vaccine against HIV remains an ongoing challenge. Protein subunit vaccines have garnered interest recently, due to desirable safety and stability profiles in comparison to whole-pathogen vaccines. However, immunization with subunit vaccines has a proclivity to elicit humoral, rather than cell-mediated, immune responses. For cytotoxic T lymphocyte (CTL) stimulation, antigenic material in the subunit vaccine must 1) be endocytosed by antigen presenting cells, 2) escape from the endosome, 3) undergo degradation by the ubiquitin proteasome pathway, and 4) be loaded onto MHC I for cross-presentation (CP) to CTLs. In this thesis, a novel vaccine is introduced that specifically targets antigens to the proteolysis pathway for amplified CP and augments endosomal escape in a nanoparticulate drug delivery platform. Inspired by proteolysis-targeting chimera (PROTAC) technologies which have been employed for *in situ* destruction of cancer-related proteins, this project explores the incorporation of a proteolysis targeting moiety (ProTM) in vaccination. We hypothesize that by conjugating an E_3 ubiquitin ligase ligand to synthetic long peptide (SLP) antigens, SLPs can be targeted for proteasomal processing and CP, ultimately resulting in improved CTL activation. Organic synthesis and click-chemistry methods were utilized to covalently modify SLPs with a ProTM. Poly(lactic-co-glycolic acid) nanoparticles that co-encapsulated the modified SLPs and the endosomal escape-promoting molecule, chloroquine, were formulated via single and double emulsion solvent evaporation. Size and loading efficiencies of nanoparticles were characterized using dynamic light scattering and absorbance. *In vitro* experiments demonstrated uptake of the ~200 nm particles by dendritic cells; quantitative colocalization analysis of fluorescently labeled SLPs and lysosomes was performed to delineate endosomal escape. With this strategy, statistically significant differences were not observed between chloroquine-containing and lacking nanoparticles. mRuby-labeled Galectin-8 cell lines were engineered for future experimental elucidation of endosomal escape. *In vivo* experiments tested the vaccine in a

prime-boost vaccination schedule, showing the highest relative antigen-specific CTL activation in the group receiving the complete formulation. The ProTM-SLP subunit vaccine technology described here can feasibly be delivered in a biodegradable, polymeric nanoparticle formulation and shows strong potential to improve cellular immune responses that are clinically relevant for vaccination against HIV and other pathogens.

Primary Reader and Advisor: Dr. Scott Wilson

Secondary Readers: Dr. Bertrand Garcia-Moreno and Dr. Kalina Hristova

Acknowledgements

I would like to express my deepest gratitude to Dr. Scott Wilson, my advisor, for his insightful guidance and feedback throughout my M.S.E. research. Dr. Wilson's thorough teaching of techniques in biomedical engineering, organic synthesis, and experimental methods provided me with relevant and translational research skills that made this endeavor possible. Joining the Wilson Lab endued me with an appreciation of immunoengineering both at the molecular scale and the broader therapeutic perspective. I would like to acknowledge all members of the Wilson Lab, and in particular, Dr. Sandeep Kumar, for his valuable instruction and counsel throughout this project. Special thanks should also go to Dr. Maxim Rosario, our collaborator, who conducted the *in vivo* mouse experiments. I would like to extend my sincere appreciation to Professor Bertrand Garcia-Moreno and Professor Kalina Hristova for serving in my thesis committee.

Contents

Abstract ii

Acknowledgements iv

List of Tables vii

List of Figures viii

1 Introduction 1

2 Background 4

2.1 Immune response to viral infection 4

2.2 HIV immunology 6

2.3 Subunit vaccines 8

2.4 Microparticles and nanoparticles 10

2.5 Current state of nanoparticle HIV vaccines 12

2.6 PROTAC 13

2.7 Endosomal disruption 14

3 Methods 16

3.1 Materials and equipment 16

3.2 Synthesis methods 17

3.2.1 VHL-DBCO 17

3.2.2 Decyl-DBCO 17

3.2.3 E3 ligase ligand and decyl conjugation to synthetic long peptides 17

3.2.4 Fluorescent labeling of SLPs 19

3.2.5 VHL-PEG-NHS 20

3.2.6 Ovalbumin-VHL ligand conjugation 21

3.3 PLGA Nanoparticle formulation 22

3.3.1 Chloroquine preparation for encapsulation 22

3.3.2 Single emulsion solvent evaporation 22

3.3.3 Double emulsion solvent evaporation 23

3.4 Nanoparticle characterization 24

3.4.1 Size 24

3.4.2 Drug loading and encapsulation efficiency 24

3.5 *In vitro* experiments 25

3.5.1 Cells 25

3.5.2 Dose-response 26
3.5.3 Investigation of chloroquine-induced endosomal escape 26
3.5.4 Microscopy 27
3.5.5 Colocalization analysis 27
3.5.6 Development of mRuby Galectin-8 cell lines 28
3.6 *In vivo* studies 29
3.6.1 Vaccination protocol 29
3.6.2 Endpoints: ELISPOT and flow cytometry 30
3.6.3 Statistical Analysis 31
4 Results 31
4.1 Nanoparticles 31
4.2 *In vitro* dose-response 32
4.3 Colocalization analysis over time 34
4.4 Engineered mRuby-Gal8 expressing DC2.4 and RAW264.7 cell lines 36
4.5 *In vivo* mouse vaccinations 39
5 Discussion and future work 40
5.1 Endosomal escape quantification by colocalization 40
5.2 Nanoparticle characterization 41
5.3 Planned *in vivo* experiments 41
5.4 Gal8-fluorescent cells for endosomal disruption analysis 42
5.5 Demonstrate therapeutic advantages of this subunit vaccine 43
6 References 45

List of Tables

Table 1. Summary of PLGA nanoparticles that were formulated and characterized.. 32

List of Figures

Figure 1. Schematic representation of the objective of this project's PROTAC-inspired vaccine design. 3

Figure 2. Mechanistic depiction of cross presentation pathways. 6

Figure 3. Progression of the traditional immune response to HIV over time without intervention. 7

Figure 4. Degradation of proteins, facilitated by PROTAC complexes. 13

Figure 5. Endosomal escape via the proton sponge effect. 15

Figure 6. Reaction scheme for the synthesis of SLP functionalized with an E3 ligase ligand. 18

Figure 7. Synthesis of SLP conjugated to a 10-carbon lipid chain for control condition formulations 19

Figure 8. Cy5 labeling of E3-functionalized SLPs. 20

Figure 9. Synthesis of NHS-functionalized VHL ligand. 20

Figure 10. Protein gel electrophoresis of VHL ligand-conjugated ovalbumin. 21

Figure 11. Emulsion solvent evaporation preparation of polymeric nanoparticles. 23

Figure 12. Vaccine schedule and groups used in the HIV CD8+ specific SLP experiment. 30

Figure 13. Representative DLS results prior to centrifugation, prior to lyophilization, and after lyophilization. 32

Figure 14. Fluorescent microscopy images acquired for the dose-response experiment 33

Figure 15. Representative images of dendritic cells dosed with particles containing Cy5-labeled SLP only and Cy5-labeled SLP with chloroquine. 34

Figure 16. Pearson correlation coefficients (PCC) with Costes thresholding over time after treatment with nanoparticles with and without chloroquine encapsulation. 36

Figure 17. Gating strategy for fluorescent activated cell sorting of positive mRuby-Gal8 cells. 38

Figure 18. ELISPOT results from in vivo experiment. 39

1 Introduction

The HIV/AIDS epidemic is one of the most pernicious global health challenges, having taken approximately 40.1 million human lives thus far [1]. Unfortunately, there is no cure, and unlike polio, measles, smallpox and hepatitis B, successful vaccination strategies against the human immunodeficiency virus are yet to be seen, despite tremendous efforts. Factors intrinsic to HIV such as the ability to form latent viral reservoirs, the infection of integral CD4+ T helper lymphocytes, and high genetic mutability contribute to the difficulty in vaccine development.

In contrast to virion-based vaccines, subunit vaccines comprising antigens and adjuvants provide better safety profiles. Traditionally, subunit vaccine platforms are biased towards elicitation of humoral, antibody-mediated immune responses. The difficulty in generation of broadly neutralizing antibodies to HIV, as well as the reduced functionality of helper T cells that facilitate B cell processes, including antibody production affinity maturation, provide motivation for an alternative prophylactic vaccination strategy. Induction of cellular immunity, executed by CD8+ T cells, is a promising avenue for cytotoxic killing of HIV-infected cells. A primary challenge in targeting CD8+ T cell activation via vaccination can be ascribed to antigen processing pathways. Upon infection by a viral pathogen, viral proteins are produced intracellularly; natural cellular processes degrade, load, and present short fragments of these proteins on major histocompatibility complex (MHC) I for presentation to cytotoxic T cells. E3 ligases facilitate the ubiquitination of proteins, targeting them for proteasomal proteolysis which generates peptides for class I MHC loading. However, antigens administered as a component of subunit vaccines are typically taken up by professional antigen presenting immune cells, then processed and presented on MHC II, eliciting the activation of CD4+ T cells. In order to initiate CD8+ T cell responses, subunit vaccine antigens must undergo cross-presentation, where extracellular antigens are endocytosed, trafficked to the cytosol, processed via the proteolysis pathway, and presented via MHC I; however, this process is

difficult to effectuate by vaccines. Here, we introduce a novel vaccine strategy that specifically targets antigens to the proteolysis pathway for enhanced antigen presentation.

Recently, proteolysis-targeting chimera (PROTAC) technologies have been clinically implemented in cancer immunotherapies. These bifunctional complexes comprise a proteolysis targeting moiety (ProTM) that recruits E_3 ubiquitin ligase, a linker, and a ligand of a protein of interest. PROTAC technologies perform by targeting specific proteins for ubiquitination and proteasomal degradation. Until now, PROTAC has been primarily used to tag cancer-related proteins existing *in situ* for subsequent destruction. This project aims to capitalize on the useful features of PROTAC in a novel capacity: to amplify peptide antigen processing for cross-presentation and activation of cytotoxic T cells. Our new vaccine is composed of peptides modified with PROTAC to target them to the proteasome for efficient processing. A nanoparticulate vaccine formulation is employed to promote uptake by antigen presenting cells (APCs). By targeting exogenous antigens for proteasomal degradation, presentation on MHC I has the potential to be enhanced (Fig. 1). We hypothesized that covalent modification of antigenic synthetic long peptides (SLPs) or whole proteins with an E3 ligase ligand will provide improved induction of cellular immunity when delivered in a nanoparticle subunit vaccine platform; co-encapsulation of a lysosomotropic agent is anticipated to promote endosomal escape and an immunostimulatory response.

In this study, we successfully demonstrated the ability to conjugate both SLPs and whole proteins to the Von Hippel-Lindau tumor suppressor (VHL) E3 ligase ligand. Furthermore, biodegradable poly(lactic-co-glycolic acid) (PLGA) nanoparticles ~200 nm in size were formulated, co-encapsulating the peptide conjugates and the endosomal escape-inducing molecule chloroquine. Validation of dendritic cell uptake of these particles was shown *in vitro* using the murine dendritic cell line DC2.4. Further *in vitro* experiments investigated the endosomal escape capabilities endowed by chloroquine by microscopic analysis of colocalization of fluorescently labeled peptides and lysosomes. Insignificant colocalization differences between particles containing and lacking chloroquine indicate that this

analytical technique may not provide sufficient sensitivity. As an alternative method, an engineered cell line expressing fluorescently labeled Galectin-8 (Gal8) proteins was developed, because Gal8 localizes to endosomes upon disruption [2]. *In vivo* experiments using Black6 and BALB/c mice were performed with a prime-boost vaccination strategy, where nanoparticle formulations were delivered along with a free CD4+ T cell targeting peptide and a PLGA-encapsulated adjuvant, the Toll-like receptor 7/8 agonist Resiquimod. These mouse studies revealed that the highest levels of CD8+ T cell-specific activation markers appeared in the group that was administered PLGA particles co-encapsulating peptide conjugated to the VHL ligand and chloroquine. These results instantiate the ability of PROTAC-based technology to elicit strong cellular immune responses that have clinical implications in the development of subunit vaccines for HIV and other infectious pathogens.

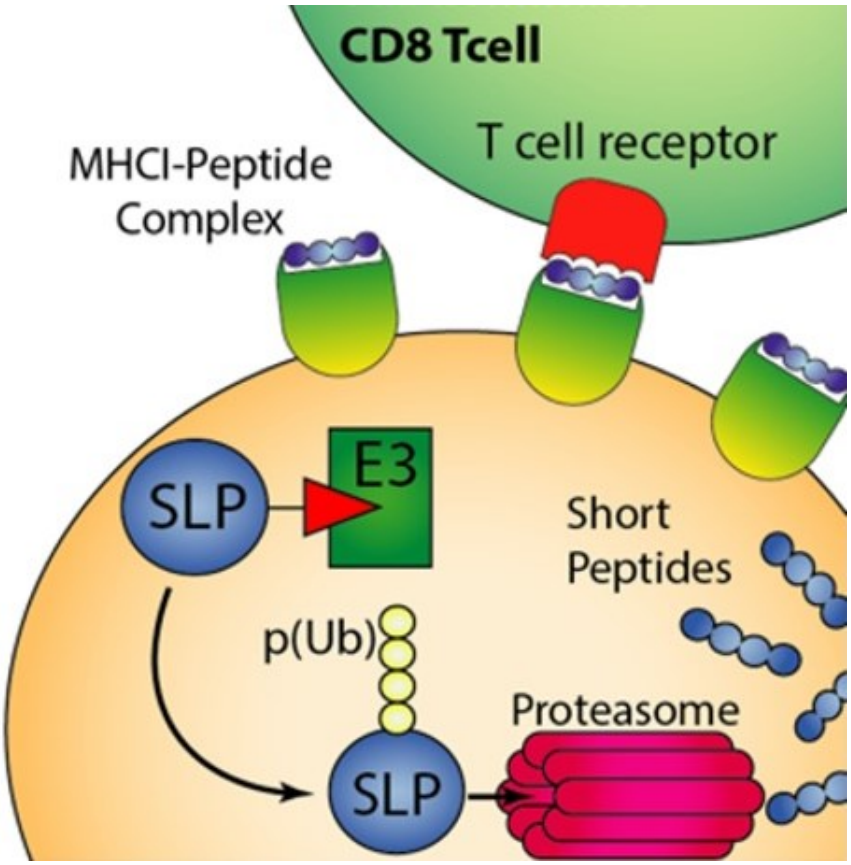

Figure 1. Schematic representation of the objective of this project's PROTAC-inspired vaccine design. A synthetic long peptide is covalently conjugated to a ligand of the E3 ligase. After cellular uptake and endosomal escape, subsequent ubiquitination targets the antigenic peptide for proteasomal degradation. Peptides are loaded onto MHC I and presented to CD8+ T cells to induce cellular immunity.

2 Background

2.1 Immune response to viral infection

Upon infection by a viral pathogen, the host must mount an effective immune response for pathogen neutralization and removal. Both innate and adaptive immunity contribute to the body's recognition of and defense against the virus. While the innate immune system proffers a rapid initial response, the adaptive immune system is crucial for long-lasting and antigen-specific protection. Immune cells arise from a hematopoietic stem cell, which develops into either a lymphoid or myeloid progenitor, giving rise to adaptive and innate cells, respectively. The adaptive immune cells are T and B lymphocytes: B cells facilitate a humoral, antibody response and T cells effectuate cellular immunity.

Immature B cells develop in the bone marrow, undergoing positive and negative selection processes involving the transmembrane B cell receptors (BCRs), which are unique to each cell. They then migrate to the spleen where they proceed to differentiate into follicular or marginal zone naïve B cells. The naïve B cells reside in secondary lymphoid organs (SLOs), including the lymph nodes and spleen, where they encounter antigens. Upon binding of a cognate antigen to its BCR, receptor-mediated endocytosis, B cell activation, and antibody secretion ensue. The B cell differentiates into proliferating plasmablasts, which immediately produce antibodies, non-proliferating and long-lived plasma cells, which secrete higher affinity antibodies after undergoing affinity maturation, and memory B cells, which are responsible for more potent responses to subsequent infections. The antigen-specific antibodies produced by B cells can address an infectious agent through several functions: they can neutralize the microbe or toxin, opsonize the microbe to be phagocytosed, facilitate antibody-dependent cellular cytotoxicity by natural killer (NK) cells, or activate the complement system, which leads to phagocytosis, inflammation, and pathogen lysis.

The second arm of the adaptive immune system comprises CD4+ (helper) and CD8+ (cytotoxic) T lymphocytes. These cells begin maturation in the thymus, where they acquire a functional T cell receptor (TCR) that is tested by positive and negative selection. The TCR enables T cells to respond to processed peptide antigens which are presented on MHC I or II. Cytotoxic T lymphocytes (CTLs) are vital due to their ability to lyse infected or tumorigenic cells directly by releasing perforin and granzyme proteins. CD4+ T cells, on the other hand, mediate the immune response by secreting cytokines. There are several types of CD4+ T cells, including Th1, Th2, Th17, T follicular helper, and regulatory T cells, each of which performs a unique role.

Antigen-presenting cells (APCs) facilitate the fundamental interplay between innate and adaptive immune cells. APCs procure a peptide antigen fragment and display it on MHC molecules to T cells. Whereas essentially all nucleated cells express MHC I, MHC II expression is limited to professional APCs like dendritic cells (DCs), macrophages, and B cells. CD8+ T cells recognize peptides 8-13 amino acids long on MHC class I; CD4+ T cells respond to 11-30 amino acid peptides on MHC class II. Classically, MHC I displays antigens of intracellular origin, and MHC II presents antigens acquired from the extracellular space. Thus, CD8+ T cells are activated against endogenous antigens in infected cells and exogenous antigens actuate CD4+ T cells. This TCR-MHC binding interaction acts as one of three signals that induce T cell activation. Additionally, co-stimulation and cytokine reception are integral to the T cell response.

Cross-presentation (CP) is the mechanism by which some professional APCs, particularly DCs, can present exogenous antigens on MHC I to CTLs. This is apposite in vaccination methods that deliver protein antigens. CP allows uptake and presentation of antigens to CD8+ T cells without requiring infection of the APC. There are two ways by which CP can occur: the cytosolic and vacuolar pathways (Fig. 2). In the vacuolar pathway, the antigen remains inside the phagosome where it is degraded and loaded onto MHC I; then, the MHC:peptide complex is transported to the cell membrane. The cytosolic pathway, in comparison, is more involved. After phagocytosis of the exogenous antigen, the antigen

must escape the endosome into the cytosol. Next, the antigen must undergo proteasomal degradation into short peptides via the ubiquitin-proteasome system (UPS). These peptide fragments are moved into the endoplasmic reticulum (ER) by transporter associated with antigen processing (TAP), loaded onto MHC I binding grooves, and relocated to the cell surface [3]. It has been shown that CP by phagocytes is more efficient with particulate than soluble immunogens [4]. In terms of the export into cytosol from the endosomal compartment, ERAD machinery, including the proteins SEC61 and p97, has been proposed to facilitate transport [5]. E3 ubiquitin ligases promote the ubiquitination of cytosolic proteins, which ultimately targets said proteins for degradation by a proteasome. When a protein is tagged with a polyubiquitin chain, the proteasome lyses it into peptides approximately 7-8 amino acids in length.

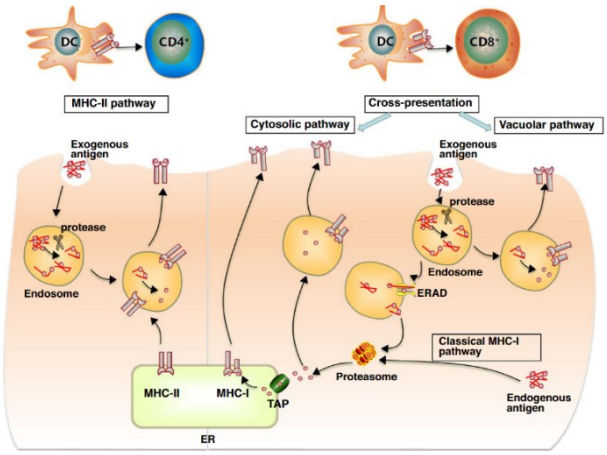

Figure 2. Mechanistic depiction of cross presentation pathways [6]. In contrast to the MHC II pathway, whereby exogenous antigens are presented to CD4+ T cells on MHC II, or the classical MHC I pathway, which enables presentation of endogenous antigens, CP facilitates the loading of exogenously sourced antigens onto MHC I for recognition by CD8+ T cells. This occurs via the cytosolic and vacuolar pathways.

2.2 HIV immunology

The HIV (human immunodeficiency virus) epidemic is a global health challenge. In 2021, 38.4 million people were living with HIV [7]. Though treatments such as antiretroviral therapy can effectively suppress the virus, latent HIV reservoirs remain, and a cure does not yet exist. HIV progresses through three stages: acute infection, chronic infection, and acquired immunodeficiency syndrome (AIDS). HIV is unusual in that it infects and depletes CD4+ T cells, thereby limiting the ability of the immune system to eradicate the virus (Fig. 3) [8]. For this reason, eliciting a robust CD8+ T cell response is critical. There is a

rare (0.5%) subset of people afflicted with HIV called elite controllers because they spontaneously suppress the virus without therapeutic intervention. Evidence points to HIV specific CD8+ T cell involvement in these elite controllers [9,10].

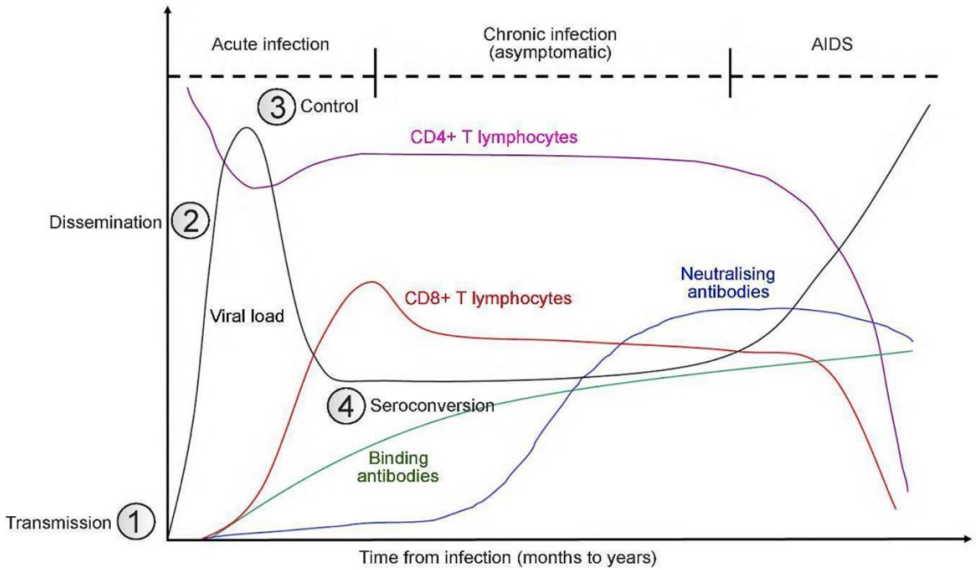

Figure 3. **Progression of the traditional immune response to HIV over time without intervention.** After infection, the acute phase is characterized by a swift spike in viral load, which then recedes to a set point. In tandem with viral load rise, CD4+ T cell numbers decrease, then increase again with the enaction of the CD8+ T cell cellular immune response. HIV specific antibodies, associated with the humoral response, begin to be produced in the acute stage. Throughout the chronic stage of HIV infection, a steady level of viraemia is maintained, and a gradual decline of CD4+ T cells occurs. Though a neutralizing antibody response is mounted, immune exhaustion eventually results in AIDS, leaving the infected host vulnerable to infections [11].

Many HIV vaccine strategies seek to generate humoral immunity, but the induction of broadly neutralizing antibodies (bnAbs) remains a challenge. The main HIV antigens that have been targeted are the CD4-binding site (CD4bs) proteins, and the proteins which form HIV envelope (Env) glycoprotein spike trimers, gp41 and gp120 [12]. However, due to high viral mutability and the fact that HIV hijacks the helper T cells, it is difficult to generate a neutralizing antibody response. An alternative approach is focused on cellular immunity. Induction of a cytotoxic effector T cell mediated response is instrumental in durable HIV control [13]. This provides the ability to target antigens with less viral escape than Env. With prophylactic immunization, CD8+ T cells could lyse HIV-infected cells and potentially clear infected cells upon initial infection to prevent reservoir formation.

2.3 Subunit vaccines

A wide variety of vaccines are in clinical use or development. Live-attenuated, inactivated, and toxoid vaccines have been in use longest, whereas viral vector, DNA, RNA, and subunit vaccines have garnered interest more recently [14]. The objective of vaccination is to generate long-lasting, adaptive immunity such that the immune system is equipped to respond sufficiently to future infection by the pathogenic agent and mitigate severe infection. In contrast to live-attenuated and inactivated vaccines which deliver whole pathogens, subunit vaccines contain only the immunogenic components. Subunit vaccines generally have a better safety profile, but the immunogenicity may be weaker, often necessitating the inclusion of adjuvants and booster doses. Subunit vaccines fall into three main classes: protein/peptide subunit, polysaccharide subunit, or glycoconjugate subunit. The first approved subunit vaccine was the hepatitis B vaccine, which delivered hepatitis B virus surface antigens (HBsAg); initially the HBsAg were acquired from infected patient plasma, but now recombinant technology is used to generate proteins [15]. In the COVID-19 pandemic, protein subunit vaccines, mRNA vaccines, and viral vector vaccines were designed against SARS-CoV-2.

Choice of protein is a critical choice in protein subunit vaccines. It is important that the elements included do not allow for pathogen reproduction but induce a robust immunogenic response. Frequently, exterior pieces of the virus capsid such as a spike protein are utilized. Neutralizing antibody responses that disable the spread of pathogens after initial infection are desired. For instance, neutralizing antibodies for HIV would block CD4+ binding or prevent fusion to the host cell membrane by targeting the CD4bs or spike proteins [16]. Broadly neutralizing antibodies (bnAbs) which can target a plethora of genetic variants of the virus are needed due to the rapid mutation rate of HIV, but development of vaccines that generate effective bnAbs remains an ongoing challenge.

One of the principal shortcomings with subunit vaccines is the proclivity to elicit humoral, but not cellular, immunity. This is because the antigenic material does not infect cells, so cytosolic immunogens

are not presented on MHC I to the cytotoxic T cells. Induction of cellular immunity by vaccines is sought-after, because CD8+ T cells can lyse infected cells and secrete tumor necrosis factor alpha (TNF-α) and interferon gamma (IFN-γ) cytokines. Recruitment of epitope-specific T cells is pertinent to infectious disease vaccine efficacy and cancer immunology.

Peptide subunit vaccines offer benefits for vaccines aimed at inducing cellular immunity. Peptides can be made synthetically, so properties such as length and amino acid sequence may be selected in a tunable manner to direct subsequent processing and presentation. Key considerations in choice of peptide sequence are that conserved epitopes are quite often subdominant, and it is important to avoid immune responses to immunodominant decoy epitopes [17]. Since T cells, unlike B cells which respond to whole protein antigens, recognize fragments of antigens loaded on MHC, the peptide structure is not a paramount consideration. T-cell epitopes are primarily dependent upon length and MHC interactions [18]. The antigen binding clefts of MHC I and II are distinct; terminal hydrogen-bonding in the MHC I cleft restricts the size of peptides loaded. For MHC I presentation, SLPs are of particular interest. When taken up by APCs, the SLPs are cleaved, loaded, and transported. Whereas SLPs for CD4+ T cell epitopes can be delivered freely for exogenous antigen loading onto MHC II, the CD8+ T cell targeting SLPs must be delivered with a mechanism for endosomal escape into the cytosol.

Immunostimulatory adjuvants are a vital element in subunit vaccines. Presence of antigenic material alone has the potential to produce a tolerogenic immune response. Activation of an immunostimulatory response is influenced by the interplay of the innate and adaptive systems. By targeting pattern-recognition receptors on APCs like dendritic cells, cytokine production can be polarized to an inflammatory response. Aluminum-based adjuvants are most common in clinically-used vaccines, and while these are efficacious for humoral immunity, alum is not ideal for cellular immunity [19]. Oil-in-water emulsions, like the FDA approved MF59, are also used to amplify APC recruitment. Monophosphoryl lipid A, part of the bacterial lipopolysaccharide endotoxin, functions as an agonist for

the Toll-like receptor (TLR) 4. Pathogen-associated molecular pattern (PAMP) recognizing TLRs, along with complement, Nod-like receptors (NLR), and C-lectin receptors (CLR) allow the innate immune system to identify infectious microbes. In humans, there are ten TLRs: some reside on the cell membrane (TLR1, 2, 4, 5, 6, and 10) whereas others are intracellular, located on the endosomal membranes and ER (TLR3, 7, 8, and 9). TLR7 and TLR8 recognize ssRNA [20]. The imidazoquinolinamine Resiquimod (R848) is a synthetic TLR 7/ 8 agonist that can modulate the immune response. When used as an adjuvant, this small molecule induces IFNα, and can promote CP [21].

An integral design aspect to subunit vaccination is the drug delivery platform. Biocompatibility, size, geometry, charge, hydrophobicity, intrinsic immunogenicity, biodegradability, and pharmacokinetic properties all must be taken into consideration. Viral vectors, virus-like particles (VLPs), ferritin cages, polymeric particles, and lipid nanoparticles can be applied as vaccine delivery platforms. These have the potential to augment biodistribution, prolong circulation times, enhance stability, and improve cellular uptake of subunit vaccines. Furthermore, targeted tissue- or cell-specific delivery is possible through incorporation of ligands, and co-delivery of multiple vaccine components can be accomplished.

2.4 Microparticles and nanoparticles

Micro and nanoparticle-based drug delivery systems have tremendous applications for subunit vaccines. Nanoparticles are materials that have at least one dimension which is less than 100 nm, while microparticles are between 0.1 and 100 μm in size. These particles can be formulated with a variety of materials, most notably lipids and polymers.

There are several reasons why nanoparticle or microparticle delivery systems are advantageous. By encapsulating therapeutic proteins or nucleic acids, nanocarriers can mitigate the degradation of therapeutic agents. Additionally, they can facilitate CP by fostering cytosolic delivery of immunogens. Particle size and charge are important factors; cationic particles are better able to provide CP due to endosomal escape abilities. Also, co-delivery of adjuvants with antigens is possible, which can bias the

immune system towards an immunostimulatory response rather than one that is tolerogenic. Additionally, nanoparticles themselves can act as adjuvants. For instance, porous silicon nanoparticles intrinsically possess adjuvant abilities, and when loaded with OVA were able to stimulate innate and adaptive immune responses [22].

Poly D,L-lactide-co-glycolide is a biodegradable FDA-approved synthetic random copolymer that has been widely used in particle synthesis. This biocompatible polymer offers substantial versatility for control of sustained drug release and particle size. Polymer molecular weight and composition (monomer ratio) can be adjusted for various applications, thereby effectuating drug release kinetics and encapsulation efficiencies. A 50:50 composition yields the most rapid degradation due to high hydrophilicity and reduced crystallinity. Upon hydrolysis, lactic acid and glycolic acid metabolite monomers are produced, which can be metabolized into CO2 and water. Furthermore, the carboxylic acid functional group can be used in reactions to modify micro or nanoparticles. A variety of methods exist for the preparation of PLGA nanoparticles, including single or double emulsion solvent evaporation, microfluidic techniques, electrospraying, spray drying, emulsification solvent diffusion, emulsification reverse salting-out, and nanoprecipitation [23]. Emulsification is the most common formulation method: single emulsification is felicitous for encapsulation of hydrophobic moieties, and double emulsifications are performed when encapsulating hydrophilic drugs or molecules.

Nanoscale particles offer attractive properties for vaccination strategies. Administration methods such as intravenous, subcutaneous, intradermal, intramuscular, and intraperitoneal injection are feasible, and accumulation in lymphoid tissues occurs due to particle size. This is pertinent for HIV therapeutic development because lymphatic organs are the sites of HIV reservoirs [24]. Lymph vessels can range from 10 µm to 2 mm in diameter. Particle sizes ranging from 20-200 nm facilitate entry into the lymphatics through endothelial cell junctions, with approximately 40 nm being the optimal size. Rather than freely entering the lymphatics, larger microparticles of 200-500 nm must be transported by

DCs. APC uptake is best with pathogen-sized particles with dimensions of 10 nm-1 μm. Size also imparts differential time courses of lymph drainage: particles under 200 nm reach lymph nodes within hours while 200-500 nm particles accumulate in lymphoid organs after 24 hours [25].

2.5 Current state of nanoparticle HIV vaccines

Nanoparticles have been employed as vehicles for HIV vaccines in a variety of ways. For example, highly active antiretroviral therapy (HAART) can be delivered in nanoparticles for long-acting slow-effective release [26]. Nanoparticles have also been used for improved delivery of latency reversal agents (LRAs) for "shock and kill" treatment strategies [24]. Targeting HIV fusion to target cells has been investigated as well; silver nanoparticles that bind gp120 can reduce infection [27]. Wei et al. reported a strategy in which polymeric nanoparticles were coated with the membrane of a CD4+ T cell: this biomimicry approach caused the HIV to bind the particles instead of the actual CD4+ T cells, consequently neutralizing the virus [28]. Another methodology for HIV treatment that makes use of nanoparticles is for genetic modification. For instance, gold nanoparticles can deliver CRISPR-Cas9 components to knock out C-C chemokine receptor type 5 (CCR5), consequently precluding HIV entry into CD4+ T cells [29]. Furthermore, nanoparticles have the capacity to improve HIV prophylaxis. Pre-exposure prophylaxis (PrEP) is an efficacious method to prevent HIV infection, but its components have short half-lives, requiring high dosages that can exacerbate adverse events. By encapsulating the drugs (tenofovir disoproxilfumarate and emtricitabine) in PLGA nanoparticles, biocompatibility and sustained release kinetics have been improved [30, 31].

Many prophylactic HIV vaccines in development focus on induction of bnAbs that target the envelope protein (Env). Murji et al. investigated a multitude of protein nanoparticle formulations which attached Env trimers from BG505 (clade A) and CZA97 (clade C) to bacterial ferritin [32]. Both single-antigen cocktails and mosaic nanoparticle immunogens demonstrated immunogenicity and neutralization in animal models. It has become evident that the ability of nanoparticles to provide

multivalent presentation of Env trimers is useful, especially in immunization priming [33]. This can be explained by the fact that avidity assists interactions between naïve B cells and immunogens, which are of relatively low affinity. One nanoparticle-based HIV therapy is the long-acting formulation of rilpivirine (RPV-LA). Rilpivirine, a non-nucleoside reverse transcriptase inhibitor, is clinically used in tandem with antiretroviral treatment: nanoparticle formulation of this drug enhanced pharmacokinetic properties [34].

2.6 PROTAC

Proteolysis-targeting chimera (PROTAC) technologies have been of interest in the last two decades, particularly for cancer immunotherapies. PROTAC is a heterobifunctional, ternary complex that includes a ligand of E3 ligase, a linker, and a ligand of a protein of interest. This conjugate promotes protein ubiquitination and degradation via the 26S proteasome in the UPS system (Fig. 4). By 2021, 15 PROTACs were in clinical use [35]. Despite the abundance of E3 ubiquitin ligases (>600), a limited number have been employed in PROTAC design. Notable ligands include Skp1-Cullin-F box complex containing Hrt1 (SCF), Von Hippel-Lindau tumor suppressor (VHL), Cereblon (CRBN), inhibitor of apoptosis proteins (IAPs), and mouse double minute 2 homolog (MDM2) [36]. The VHL E3 ligase is recruited to Hypoxia-Inducible Factor 1 α (HIF1-α) degron motif upon hydroxylation of Pro residues [37].

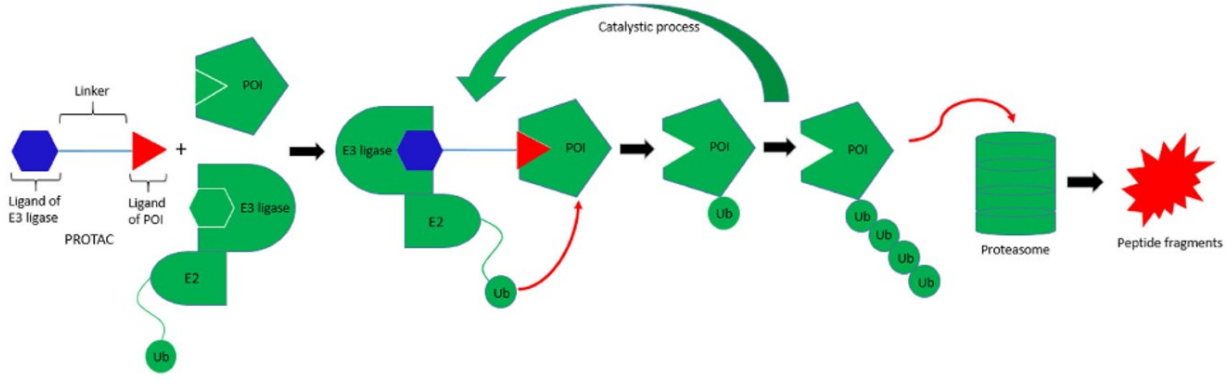

Figure 4. Degradation of proteins, facilitated by PROTAC complexes [36]. The bifunctional PROTAC is composed of a ligand for a protein of interest (POI), linked to a ligand for E3 ligase. Connection of the POI with E3 ligase mediates ubiquitination of the POI, ultimately resulting of proteasomal degradation.

PROTAC has implications in anticancer therapies due to its ability to reduce the quantity of disease-relevant proteins. Further, PROTACs have sub-stoichiometric catalytic activity and can be reused for multiple cycles of protein degradation [38]. An example of a PROTAC use was reported by Maneiro et al.: a trastuzumab-PROTAC conjugate was able to trigger degradation of bromodomain containing protein 4 (BRD4) selectively in human epidermal growth factor receptor 2 (HER2) positive breast cancer cell lines [39]. Recently, there have been many advances in PROTAC technology, including the development of in-cell click-formed proteolysis-targeting chimeras (CLIPTAC), photochemically targeted chimera (PHOTAC), Semiconducting polymer nano-PROTAC (SPNpro), Floate-PROTAC, Antibody PROTAC conjugate and antibody-based PROTAC (AbTAC), Ribonuclease targeting chimeras (RIBOTACs), Transcription factor-PROTAC (TF-PROTAC), and Chaperone-mediated protein degradation (CHAMP) [40]. An interesting design, termed opto-PROTAC, was reported by Liu et al.; this incorporated a light-inducible switch to endow PROTACs with spatiotemporal control [41].

2.7 Endosomal disruption

A salient process in nanoparticle delivery platforms is escape from the endosomal compartment into the cytosol. There are multiple mechanisms by which cells internalize extracellular material, such as phagocytosis, caveolar-dependent endocytosis, clathrin-dependent endocytosis, and actin-dependent micropinocytosis. Upon endocytosis, the material is trafficked to the trans-golgi network, to the plasma membrane, or to lysosomes where degradation occurs. In comparison to the cytoplasmic pH of ~7.0, the pH within the vesicle drops from ~6.5 in the early endosome (EE) to ~5.5 in the late endosome (LE) and later to ~4.5 in the lysosome, due to proton pump regulation [42]. Proteins can be used as markers to characterize these compartments in the endocytic pathway: Rab5, Rab7, and LAMP1 are associated with EEs, LEs, and lysosomes, respectively.

For subunit vaccine drug delivery, efficient endosomal escape is essential; to this end, lysosomotropic agents are frequently used. These chemicals function by diminishing the physiological pH gradient between endosomes and the cytosolic space. Osmosis leads to swelling and disruption of the endosomal/lysosomal membrane, releasing the components (Fig. 5). Among the lysosomotropic agents, chloroquine and its derivatives are most frequently used: this diprotic weak base can counteract endosomal acidification. As chloroquine is protonated during endosome maturation, water and chloride ion influx results in endosomal rupture, a process which has been termed the 'proton sponge effect' [43]. For most cell types, >100 µM chloroquine concentration is required to induce endosomal disruption [44].

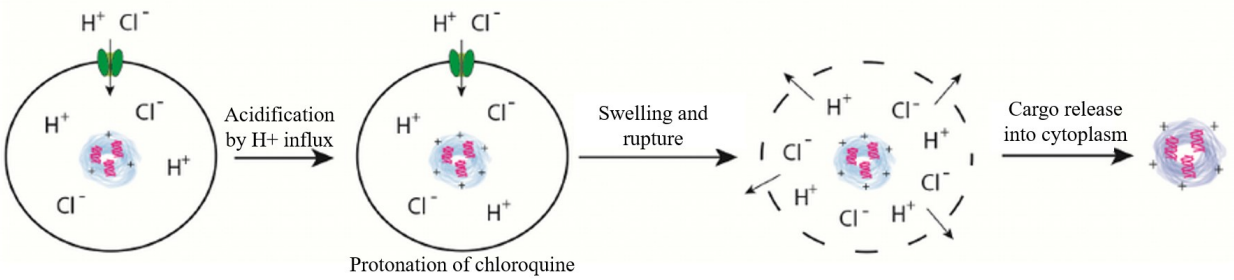

Figure 5. Endosomal escape via the proton sponge effect. Incorporation of a lysosomotropic agent can promote escape from the endosome into the intracellular cytosolic space. The delivered drug formulation is first endocytosed by the cell; then, natural ATP-ase activity facilitates acidification within the endosome. When lysosomotropic agents – such as the weak base chloroquine – are included, proton influx is buffered. Influx of chloride ions and water molecules results in swelling and rupture of the endosomal membrane, and the cargo is released into the cytosolic space. Figure adapted from Agirre et al. [45].

An alternative method to promote endosomal escape, which also relies upon the proton sponge effect, is use of pH-responsive polymers. For example, polyethylenimine (PEI) polymers and polyamidoamine (PAMAM) dendrimers comprise secondary and tertiary amines that can serve as buffers in endosomal acidification [44]. Yang et al. reported a poly-L-lysine (PLL) coating on their gold nanoparticles that was able to disrupt endosomal membranes, enabling cargo escape from EEs and LEs [46].

3 Methods

3.1 Materials and equipment

Poly(D,L-lactide-co-glycolide) (50:50 lactide/glycolide ratio; M_w 7,000-17,000), Resiquimod, decylamine, choroquine diphosphate, Dibenzocyclooctyne-N-hydroxysuccinimidyl ester, (S,R,S)-AHPC-PEG3-NH2 hydrochloride, N3-PEG3500-NHS, poly(vinyl alcohol) (PVA), molecular biology-grade sucrose, and poly-L-lysine were purchased from Sigma-Aldrich (St. Louis, MO). Cy5-NHS ester was purchased from BroadPharm (San Diego, CA). Dichloromethane (DCM), dimethyl sulfoxide, dimethylformamide, and methanol were purchased from Thermo Scientific (Waltham, MA). EndoFit™ Ovalbumin and Lipofectamine™ LTX Reagent with PLUS™ Reagent were purchased from InvivoGen. Mini-PROTEAN® TGX™ Precast Gels from Bio-Rad (Hercules, CA) and SimplyBlue™ SafeStain from Invitrogen (Waltham, MA) were used for protein conjugation analysis; Ziba Spin Desalting Columns from Thermo Scientific (Waltham, MA) were used for protein purification. Cell culture chamber slides (8-well, Cat. #: 230128) purchased from NEST Scientific (Woodbridge, NJ) were used for *in vitro* experiments. For cell fixation, a 4% w/v paraformaldehyde solution in PBS was prepared with paraformaldehyde powder from Sigma-Aldrich (St. Louis, MO). Immuno Mount DAPI and DABCO Mounting Media was purchased from Avantar (Radnar, PA). The Malvern Panalytical Zetasizer was used for Dynamic Light Scattering size measurements (Westborough, MA) and the Thermo Scientific NanoDrop Spectrophotometer was used for absorbance measurements (Waltham, MA). High performance liquid chromatography (HPLC) measurements were performed with the Jasco HPLC (Easton, MD). PB-CAG-mRuby3-Gal8-P2A-Zeo was a gift from Jordan Green (Addgene plasmid # 150815; http://n2t.net/addgene:150815; RRID:Addgene_150815). Cell sorting was performed using the Beckman-Coulter MoFlo XDP Cell Sorter (Brea, CA). Custom peptides with terminal azide groups ((Azide)KDVSGLEQESIINFEKLAAAAAC-OH (2433 g/mol) and (Azide)LKDPVHGVYYDPSKDLIAEIQYWQA-OH (3206.7 g/mol)) were synthesized by the

Synthesis and Sequencing Core Facility at the Johns Hopkins School of Medicine. Image analysis and quantification was achieved using Fiji software and the JaCoP plugin.

3.2 Synthesis methods

3.2.1 VHL-DBCO

The von Hippel-Lindau (VHL)-recruiting ligand (S,R,S)-AHPC-PEG3-NH2 was functionalized with dibenzocyclooctyne (DBCO). (S,R,S)-AHPC-PEG3-NH2 (37 mg, 0.059 mmol) was solubilized in 0.5 mL of dimethylformamide (DMF) with triethylamine (TEA) (16.5 uL, .118 mmol). DBCO-NHS ester (50 mg, 0.124 mmol) dissolved in 0.2 mL DMF was added dropwise to the stirred mixture at 0° C (Fig. 6). After 1 h, the reaction mixture was reacted further at room temperature (rt) for 24 h. DMF was removed *in vacuo* (IKA rotary vacuum evaporator), and the product was resolubilized in dichloromethane (DCM). Preparatory thin layer chromatography (TLC) was performed in a chamber containing methanol:DCM solvent system (2:23) for purification; the TLC plate bands were visualized under 254 nm UV light. The product in silica was extracted and purified via flash chromatography with a 10:90 methanol:DCM solvent system to obtain a 72.26% yield (41.3 mg). Synthesis of the desired product was confirmed by ^{1}H NMR.

3.2.2 Decyl-DBCO

For use as an experimental control, DBCO-functionalized n-decane was synthesized. Decylamine (99.34 uL, .497 mmol) was stirred in 1 mL DCM with TEA (69 uL, .497 mmol, pH 9). DBCO-NHS ester was added dropwise (100 mg, .249 mmol) and the reaction mixture was stirred for 24 h (Fig. 7). Purification by prep TLC yielded 46 mg (41.55%) of product which was confirmed by ^{1}H NMR.

3.2.3 E3 ligase ligand and decyl conjugation to synthetic long peptides

The DBCO-functionalized VHL ligand was conjugated to SLPs functionalized with a terminal azide group via a copper-free cyclic alkyne click-chemistry reaction (Fig. 6). Both SIINFEKL

(Azide)KDVSGLEQESIINFEKLAAAAAC-OH (2433 g/mol) and CD8+ T cell (Azide)LKDPVHGVYYDPSKDLIAEIQYWQA-OH (3206.7 g/mol) targeting peptides were used. Conjugations using 2-5 mg of SLPs and of VHL-DBCO (1.2 equivalents) were performed under sterile conditions in 100 uL DMF for 1 h at rt, as schematically depicted.

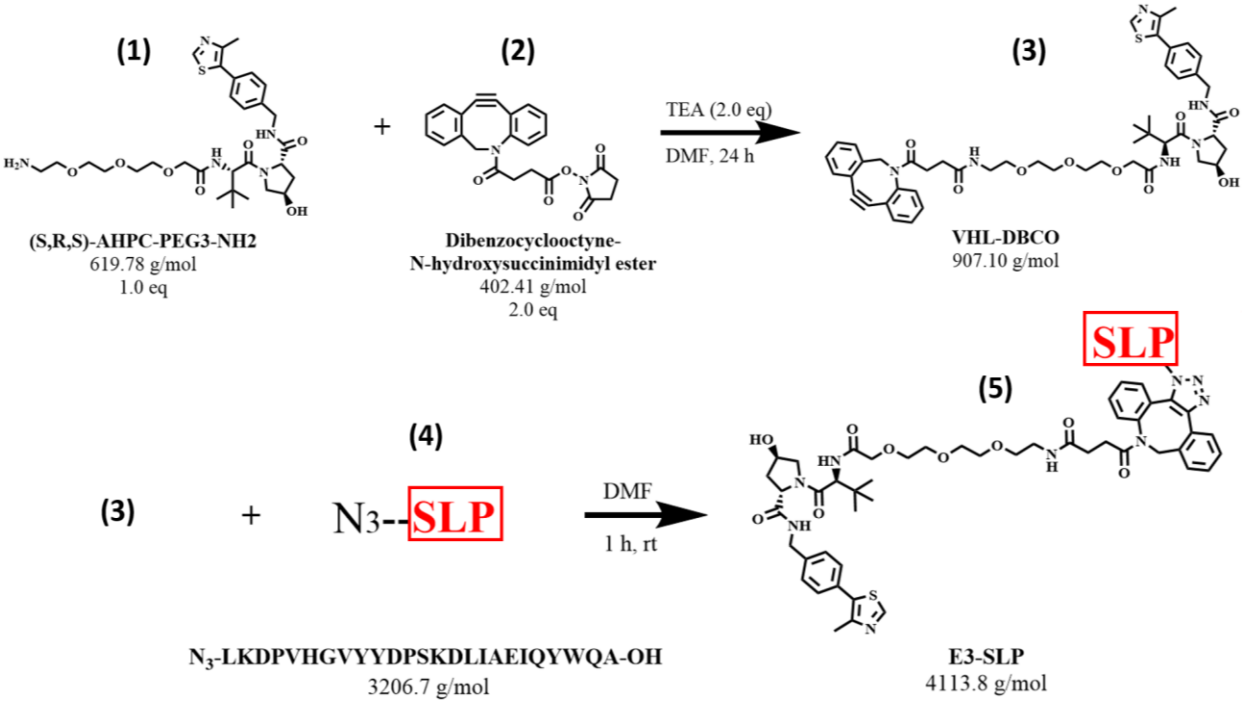

Figure 6. Reaction scheme for the synthesis of SLP functionalized with an E3 ligase ligand. First, the von Hippel-Lindau (VHL)-recruiting ligand (S,R,S)-AHPC-PEG3-NH2 was functionalized with a cyclic alkyne moiety in basic conditions. After purification, the product underwent click-chemistry with the azide-terminated peptide.

The (Azide)LKDPVHGVYYDPSKDLIAEIQYWQA-OH SLP was covalently conjugated to decyl-DBCO (Fig. 7). Addition of the lipid chain was theorized to be a superior control to the unconjugated N_3-SLP alone for two reasons: the product is akin to an inert VHL ligand conjugated peptide, and the hydrophobic character endowed by decane improves encapsulation efficiency of the peptide in nanoparticles. The conjugation was carried out in 100 uL DMF at rt. Products were precipitated in acetone and reconstituted in DMF for stock solutions that were stored at -20 °C.

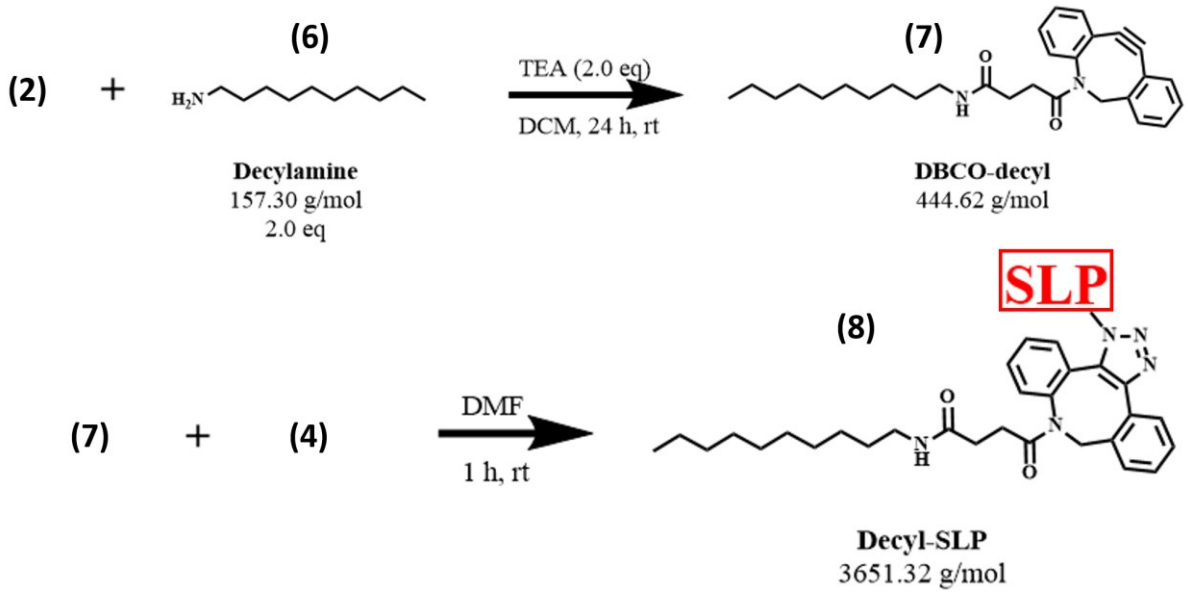

Figure 7. Synthesis of SLP conjugated to a 10-carbon lipid chain for control condition formulations. Decylamine was reacted with the amine reactive DBCO-NHS ester at pH 8. The DBCO-decyl product and the azide-functionalized peptide were reacted and the cyclic alkyne-azide click-chemistry reaction yielded peptides with an attached alkyl chain.

3.2.4 Fluorescent labeling of SLPs

For use in *in vitro* experiments, VHL ligand conjugated SLPs were fluorescently labeled with Cy5. Cy5-NHS ester was used for its hydrophobicity, because good solubility in DCM was a requisite for adequate nanoparticle encapsulation. Cy5-NHS ester was reacted in DMF with primary amines present in the SLP's lysine residues in the presence of a small amount of TEA (4 uL, pH 8) (Fig. 8). The Cy5-labeled peptide product was precipitated in acetone.

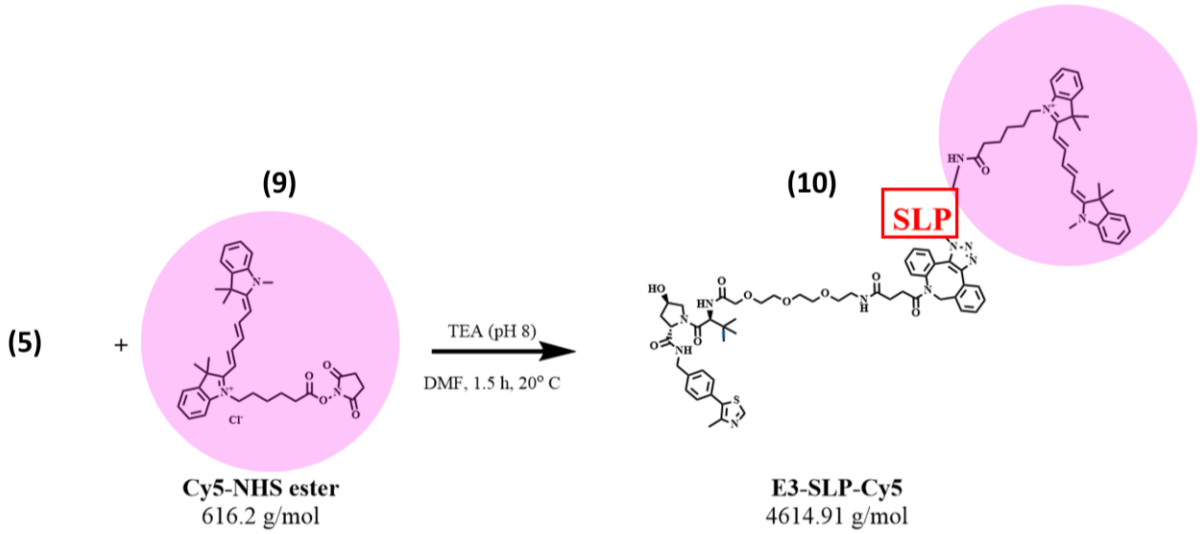

Figure 8. Cy5 labeling of E3-functionalized SLPs. Under basic conditions, commercially available Cy5-NHS was reacted with the VHL ligand functionalized peptides. Primary amines present on the two lysine residues of the peptides reacted with the NHS ester, producing fluorescently labeled peptides for nanoparticle formulations used in *in vitro* experiments.

3.2.5 VHL-PEG-NHS

To be used in the conjugation of the VHL ligand to whole ovalbumin (OVA), an NHS functionalized VHL ligand with a polyethylene glycol (PEG) linker was synthesized. An azide-cyclic alkyne click-chemistry reaction was carried out between NHS-PEG(3500)-N_3 (25.5 mg, 0.00728 mmol) and VHL-DBCO (6 mg, 0.00662 mmol) for .5-1 h in anhydrous DMF (Fig. 9). The product was precipitated in ether and fully dried.

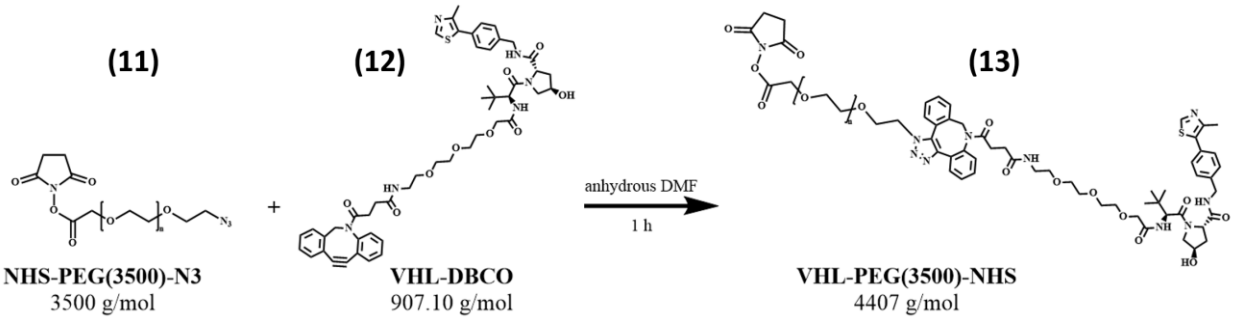

Figure 9. Synthesis of NHS-functionalized VHL ligand. A 3500 g/mol PEG linker with terminal NHS ester and azide groups was reacted in anhydrous DMF with the DBCO-functionalized VHL ligand. Care was taken to keep the VHL-PEG-NHS product in the absence of water to mitigate potential cleavage of the NHS functional group.

3.2.6 Ovalbumin-VHL ligand conjugation

VHL-PEG-NHS was conjugated under sterile conditions to endotoxin-free OVA protein in a 30:1 molar ratio. OVA was first reconstituted in PBS at a 50 mg/mL concentration. A phosphate buffer solution was added (10% total volume) to reach a pH 7.8. The VHL-PEG-NHS product was dissolved in minimal DMF such that the DMF volume was less than 10% of the PBS volume and then added dropwise to the rapidly stirring solution of OVA. The reaction was allowed to proceed for 4 h.

Conjugation was assessed by running equivalent masses of OVA and OVA-PEG-VHL on a precast Mini-Protean gel (Fig. 10). Staining with Coomassie blue provided visualization of conjugation progression. The conjugated protein solution was then purified using Zeba columns. High-performance liquid chromatography (HPLC) was used for analytical determination of protein conjugation.

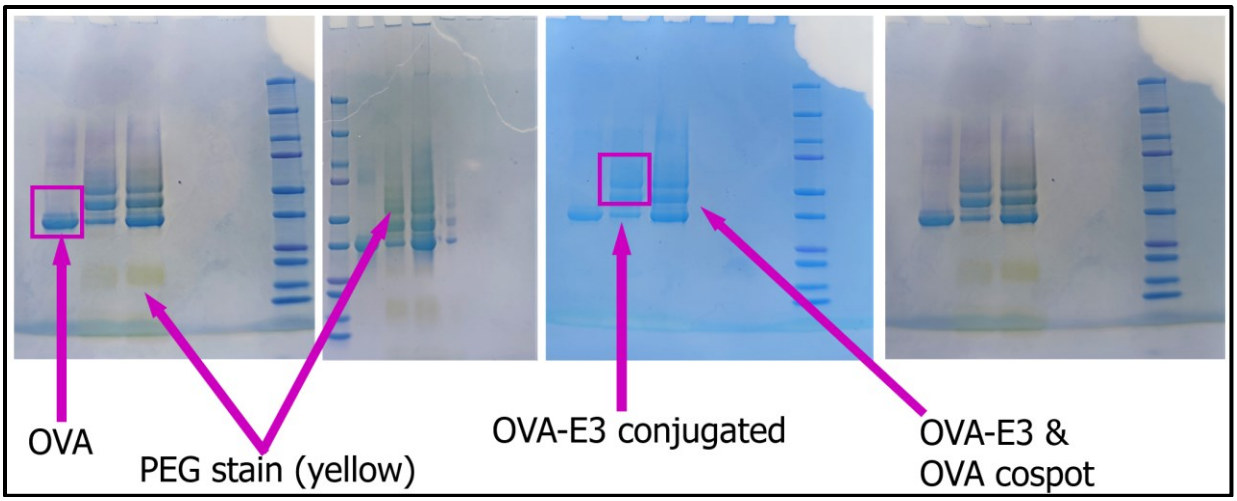

Figure 10. Protein gel electrophoresis of VHL ligand-conjugated ovalbumin. Conjugation of the VHL ligand to endotoxin-free ovalbumin was assesed with gel electrophoresis. The conjugation reaction mixture was monitored in comparison to unconjugated stock ovalbumin. Staining with Coomassie blue provided visualization of separate bands on the gel associated with conjugated protein. Furthermore, a barium iodide stain revealed the presence of the PEG linker on conjugated proteins.

3.3 PLGA Nanoparticle formulation

3.3.1 Chloroquine preparation for encapsulation

In order for chloroquine to be efficiently encapsulated in PLGA nanoparticles, it was crucial that it be hydrophobic. Since commercially available chloroquine diphosphate salt is water-soluble, it was solubilized in DMSO in the presence of 2.2 equivalents TEA with stirring overnight. This solution was centrifuged at 1500 G for 4 min, and the supernatant was filtered to obtain a stock solution of chloroquine in DMSO. A standard dilution curve of chloroquine diphosphate absorbance was used to calculate the chloroquine concentration in the stock solution.

3.3.2 Single emulsion solvent evaporation

Particles encapsulating hydrophobic components were formulated using a classical single emulsion (oil/water) method under sterile conditions (Fig. 11). 50 mg PLGA (7-17k) was dissolved in 2 mL anhydrous DCM in a glass 20 mL vial. Chloroquine (4 mg) and SLP conjugates (typically 2-4 mg) were added to the solution. Particles containing only the adjuvant R848 were also synthesized using the single emulsion method. 2 mL of 5% poly(vinyl alcohol) (PVA) in DI water was added to the vial, and probe sonication was utilized to form the emulsion (40 s, 30% amplitude). The emulsion was then quickly pipetted dropwise into a preheated, stirring 30 mL solution of 1% PVA in DI water (50° C, 1100 rpm). After 3 h, the solution was transferred to a 50 mL tube and centrifuged for 25 min at 11,000 G. The supernatant was decanted, and the nanoparticles were washed with DI water and centrifuged again. Particles were resuspended in 5 mL DI water containing 10 mg sterile sucrose, a lyoprotectant, and lyophilized. Sterile conditions were maintained, and particles were stored at -20° C.

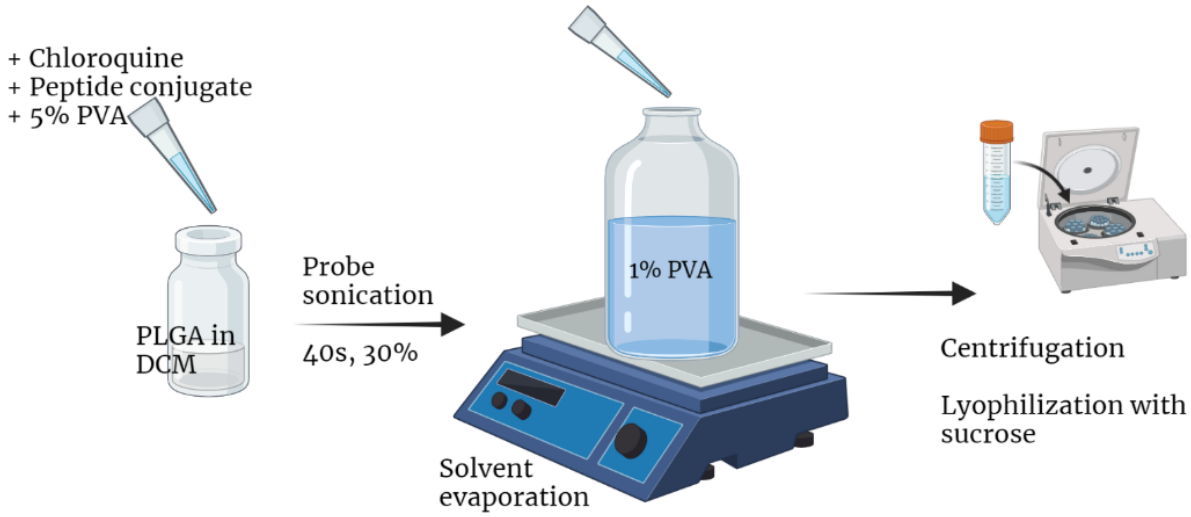

Figure 11. Emulsion solvent evaporation preparation of polymeric nanoparticles. Organic and aqueous liquid phases with dissolved PLGA, CQ, and peptide conjugates were probe sonicated. The emulsion was immediately added to stirring 1% PVA solution. After solvent evaporation, particles were harvested by ultracentrifugation and freeze-dried. *Created with BioRender.com.*

3.3.3 Double emulsion solvent evaporation

Double emulsion (w/o/w) solvent evaporation was also employed for nanoparticle formulation; this method was advantageous for the encapsulation of hydrophilic compounds. Water-soluble components localize in the hydrophilic core and hydrophobic molecules are loaded in the PLGA shell. A 400 uL buffer solution of 50% acetonitrile (ACN) and 50 mM HEPES was prepared, into which peptide or ovalbumin conjugates were mixed. The first emulsion was formed by adding this solution to 50 mg PLGA dissolved in 2 mL DCM and probe sonicating for 40 s at 30% amplitude. The primary emulsion was then added to 2 mL 5% PVA and sonicated at 30% for 40 s. In the same manner as the single emulsion solvent evaporation, this was added dropwise with rapid stirring to a preheated 1% PVA solution. After 3 h, the nanoparticles were harvested as described above.

3.4 Nanoparticle characterization

3.4.1 Size

Dynamic light scattering (DLS) was used to determine particle size. DLS measurements of particles suspended in DI water were acquired prior to centrifugation, before lyophilization, and after lyophilization.

3.4.2 Drug loading and encapsulation efficiency

Characterization of drug loading is critical for matching doses in experiments and optimizing encapsulation efficiencies (Eqn. 1). The drug loading was found through absorbance measurements. First, standard dilution curves in DMSO were made for chloroquine, R848, and each unique peptide conjugate for their peak absorbances. Chloroquine was measured at the wavelengths 260, 280, and 338 nm; Cy5 peptide absorbance was recorded at 647 nm, R848 was recorded at 325 nm, and conjugated peptides were measured at 280 nm.

Equation 1. Encapsulation efficiency calculation. Drug loading is calculated as the ratio by dry mass of drug in nanoparticles. The encapsulation efficiency is the proportion of drug encapsulated in particles to the total drug used in formulation.

$$Encapsulation\ Efficiency\ (EE\%) = \frac{mass\ of\ drug\ in\ nanoparticles}{mass\ of\ drug\ used\ in\ formulation} * 100$$

From each batch of lyophilized nanoparticles, at least three samples of approximately 2 mg were precisely weighed out. The PLGA particles were digested in dimethyl sulfoxide (DMSO) at a concentration of 1 mg/100 uL with bath sonication. Sample absorbances were recorded with a NanoDrop spectrophotometer. Using the standard dilution curves, component concentrations could be interpolated. Due to spectral overlap of chloroquine and peptides at 280 nm, samples of nanoparticles which co-encapsulated chloroquine required additional calculations. Absorbance at 338 nm was used to find chloroquine concentration, and the expected chloroquine concentration at 280 nm was subtracted

from the measured absorbance. This absorbance differential was then used to calculate peptide concentration.

HPLC was also used to analyze the component amounts within nanoparticles, including particles which encapsulated ovalbumin protein. A DMSO/NaOH/SDS procedure developed by Sah was applied to solubilize PLGA microspheres and proteins in a single phase [47]. In short, accurately weighed PLGA particles were dissolved in 1 mL DMSO for 1 h, and then a 5 mL 0.05 N NaOH solution with 0.5% w/v SDS was added, mixed, at incubated at rt for 1 h. The filtered solution was then run on HPLC and compared against standards to quantify drug loading.

3.5 *In vitro* experiments

3.5.1 Cells

Murine dendritic DC2.4 cells (ATCC; Manassas VA) were cultured under sterile conditions at 37° C with 5% CO_2. RPMI-1640 + Glutamax growth medium with 10% fetal bovine serum (FBS), 1X non-essential amino acids, 1X HEPES buffer solution, 1X penicillin/streptomycin, and 0.0054X β-Mercaptoethanol was used. After washing with PBS, subcultured cells were lifted with 0.25% Trypsin/EDTA, resuspended in growth media, counted using a 1:1 mixture of homogeneous cell suspension and 0.4% Trypan Blue stain, and plated at a density of 5 x 10^4 cells/well in 8-well chamber slides 24 hours prior to treatment. Prior to cell plating, the chamber slides were treated with 0.1% w/v poly-L-lysine for 5 min and rinsed with PBS to aid in cell adherence.

For development of cell lines expressing fluorescently labeled galectin-8 (Gal8), macrophage RAW264.7 (ATCC; Manassas VA) were used in addition to DC2.4s. DMEM growth medium with 10% FBS was used for cell culture, and cells were subcultured using a standard cell scraping technique.

3.5.2 Dose-response

An initial dose-response experiment was performed to determine appropriate nanoparticle treatment amounts. PLGA nanoparticles containing either fluorescently labeled Cy5-SIINFEKL-E3 or Cy5-CD8pep-E3 and chloroquine were utilized. Immediately before treatment, particles were resuspended with bath sonication and vortexing in PBS to create stock solutions at several concentrations. Concentrations tested included 0.2, 0.15, 0.1, 0.05, 0.01, 0.005, and 0.0025 mg/mL, which equated to 0.05, 0.0375, 0.025, 0.0125, 0.0025, 0.00125, and 0.000625 mg particles per well. Media was aspirated from the chamber slide wells and replaced with 250 µL fresh complete growth media. Cells were incubated after application of NP suspensions for 4 h, then washed and covered with fresh media. A treatment time of 4 h was selected because nanoparticles have been shown to enter early endosomes within 2 h and uptake saturates at 4 h, then declines [48]. After 12 h, cells were fixed with 4% PFA for 20 min and washed with PBS. The chamber was removed from the slide and Immuno Mount DAPI and DABCO Mounting Media was applied prior to sealing with a cover slide.

3.5.3 Investigation of chloroquine-induced endosomal escape

To examine the impact of including chloroquine in particle formulations, *in vitro* experiments were conducted testing a range of time periods (6 – 72 h) between treatment and fixation. The particles containing fluorescently labeled peptides with and without chloroquine were suspended in PBS at 2.5 mg/mL concentrations. As described above, wells were aspirated and replaced with 250 µL complete growth medium 24 h after plating. Each treatment well received 5 µL of nanoparticle suspension (0.0125 mg) for 4 h prior to washing. Two hours prior to fixation, 1X Lysoview GFP dye was applied to stain the lysosomes of live cells. 4% PFA was used to fix cells, which were then washed and prepared for imaging with DAPI-containing mounting media. Experimental controls included cells not stained with Lysoview dye, cells not treated with nanoparticles, cells stained only with free chloroquine (450 µM), and free chloroquine vortexed and administered with the peptide-only particles.

3.5.4 Microscopy

The Zeiss AxioObserver.Z2 (with Apotome) inverted microscope was used for image acquisition. Zeiss filter cubes 49, 38, and 50 were used for DAPI, GFP, and Cy5 signals, respectively. Consistent settings were used for each experimental condition at 63x magnification with oil immersion. Exposure times of 70 ms, 300 ms, and 1000 ms were used for DAPI, EGFP, and Cy5 channels, respectively. Image files were processed and analyzed using Fiji software.

3.5.5 Colocalization analysis

To investigate the endosomal escape properties imparted by chloroquine, colocalization of lysosomes and fluorescently labeled SLPs was quantified. EGFP (Lysoview dye signal) and Cy5 (peptide) channels from the 63x images were imported into Fiji software. The JACoP plugin (Just another colocalization plugin) was employed for colocalization quantification. Key metrics such as the Pearson correlation coefficient (PCC) with Costes threshold and Mander's correlation coefficients were calculated in an automated fashion.

PCC is a statistic that measures the pixel-by-pixel signal covariance in two images. Since the mean intensity is subtracted from each pixel, this value is independent of background and overall intensities. PCC is frequently used due to its facileness; extensive preprocessing is unnecessary [49]. A negative control can be produced by rotating one of the two images by 90 degrees. A method was developed by Costes et al. to estimate threshold values to use in a reproducible and automatable manner [48]. The Costes method distinguishes fluorescently labeled molecules from background signal through an analysis which finds the pixel value range that results in a positive PCC. The Costes method is advantageous because it eliminates user bias and has been implemented in many ImageJ colocalization plugins. A distinct set of quantifiable metrics of colocalization are the Manders' Colocalization Coefficients (MCC), each of which describes the fraction of one signal that colocalizes with a second signal [50]. For the purposes of this research, MCC calculates the fraction of Cy5 signal in pixels

containing Lysoview dye GFP signal from the other channel, and the fraction of GFP Lysoview dye signal in pixels containing Cy5. In contrast to PCC, which is influenced by proportionality of signal intensities, MCC is solely a measure of co-occurrence.

3.5.6 Development of mRuby Galectin-8 cell lines

Multiple strategies have been published for visualization and quantification of endosomal/lysosomal escape. A traditional qualitative assay for endosomal rupture is calcein, which diffuses from endosomes to cytosol upon rupture [51]. Fluorescent probes can be used to stain endosomal compartments, such as with Lysotracker dyes as described above. Yet another strategy is to genetically engineer a cell line. Galectin proteins have been demonstrated to localize to endocytic vesicles upon membrane disruption. Previously, du Rietz et al. investigated endosomal release of siRNA that was instigated by the vesicle-disrupting drugs chloroquine, siramesine, and amitriptyline treatment, using cells stably expressing YFP-tagged galectin-1, -3, -8, and -9. The galectin recruitment events were tracked over 24 h by live-cell imaging with a confocal laser scanning microscope [2]. Tracking Gal8, a β-galactoside carbohydrate-binding protein, offers benefits over other methods used to assess endosomal disruption, such as the ability for high-throughput screening of drug delivery systems. When using colocalization of fluorescent cargo and Lysotracker dyes, supra-therapeutic doses may be necessitated for adequate colocalization analyses due to the sensitivity limitations of microscopy, and fixation artifacts can confound results [52]. Since the choices of exposure settings are generally biased toward the brightest fluorescence signals, these may detect only the concentrated signals in the endosomes and mask the lower cytosolic signals.

For this study, dendritic and macrophage cell lines fluorescently expressing mRuby-Gal8 were developed. PiggyBac transposon-based DNA integration was utilized to transfect cells with PB-CAG-mRuby3-Gal8-P2A-Zeo (Plasmid #150815, gifted by Dr. Jordan Green's lab). The PB-mRuby-Gal8 transposon and PB-Transposase plasmids were combined in a 6:1 mass ratio, and a commercially

available Lipofectamine LTX transfection kit was used to transfect DC2.4 and RAW264.7 cells which had been plated 24 h prior at 6.2 x 10^4 cells/well in a 48-well plate. Fluorescence activated cell sorting (FACS) was performed 8 days later to sort and isolate mRuby-positive cells.

3.6 *In vivo* studies

3.6.1 Vaccination protocol

For *in vivo* mouse experiments Black6 and BALB/c mice were used for SIINFEKL and CD8 peptide studies, respectively. Mice were vaccinated in a prime-boost design, where a pDNA prime was administered at day 0, and nanoparticles were injected as a boost at day 21, as depicted in Figure 12. Injection volumes of 80 uL were used for resuspended nanoparticles.

For the SIINFEKL experiment, 30 ug R848 that was encapsulated in PLGA nanoparticles and 24 ug SIINFEKL peptide was administered per mouse (n = 4). Group 1 received nanoparticles that encapsulated the VHL ligand-conjugated SIINFEKL SLP, and group 2 was treated with free VHL ligand-conjugated SIINFEKL.

In the first CD8 SLP experiment, BALB/c mice were divided into 5 groups for injections (n = 3). All groups (n = 3) received 100 ug free CD4-targeting peptide antigen. Group 1 was administered VHL-conjugated peptide in nanoparticles and R848 in nanoparticles; group 2 was treated with VHL-conjugated peptide and chloroquine co-encapsulated in particles; group 3 was treated with VHL-conjugated peptide and chloroquine co-encapsulated in nanoparticles and R848 in nanoparticles (full formulation); group 4 was given unconjugated peptide and chloroquine co-encapsulated in nanoparticles and R848 in nanoparticles; group 5 was injected with R848 particles and free VHL-conjugated peptide.

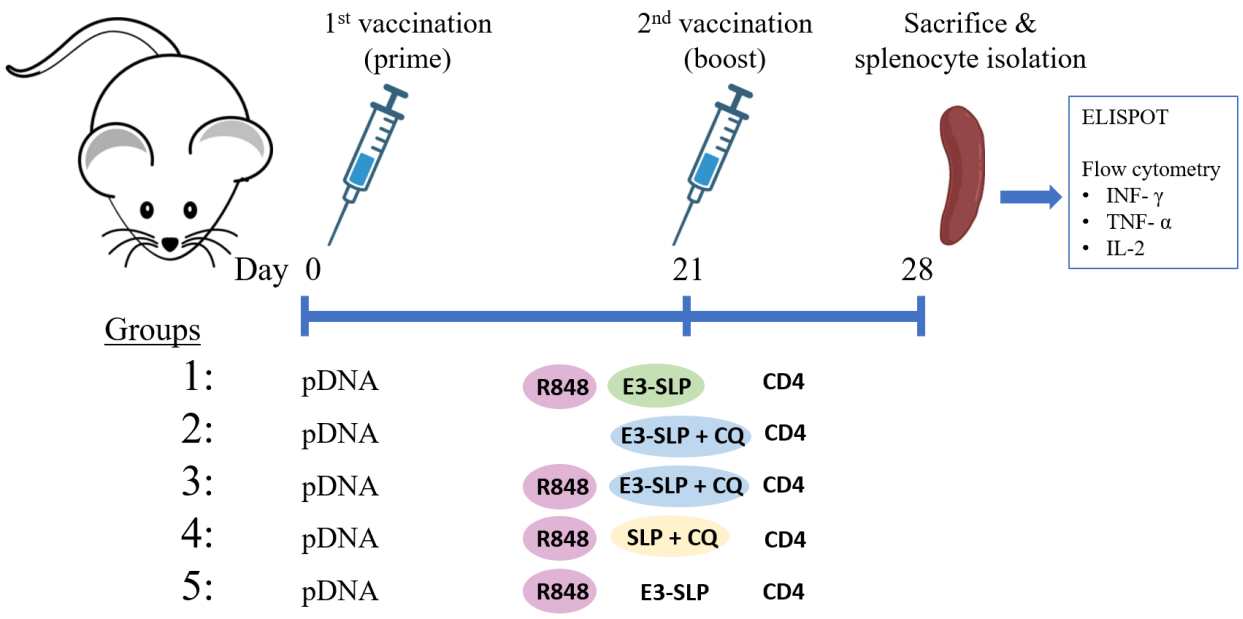

Figure 12. Vaccine schedule and groups used in the HIV CD8+ specific SLP experiment. A DNA prime was administered to all groups at day 0. Each group received CD4 targeting SLPs along with a unique formulation at day 21. The full formulation (R848 particles, and particles co-encapsulating VHL ligand-conjugated peptides and chloroquine) was injected in the group 3 mice; other groups served as controls for R848, chloroquine, and SLP alone. Upon experiment conclusion, the mice were sacrificed and isolated splenocytes were assayed with ELISPOT and flow cytometry, n=3.

For the second CD8 SLP experiment, all groups (n = 3) received 100 ug free CD4-targeting peptide antigen and 50 ug R848 encapsulating PLGA nanoparticles per mouse. Group 1 was only administered the CD4 and R848; group 2 also received 40 ug CD8-targeting peptide that was conjugated to the VHL ligand and encapsulated in particles; group 3 also received 40 ug CD8-targeting peptide that was conjugated to the VHL ligand and co-encapsulated with chloroquine in particles.

3.6.2 Endpoints: ELISPOT and flow cytometry

At the completion of the experiments, mice were sacrificed. Splenocytes were isolated and assayed by ELISPOT and flow cytometry for INF- γ, TNF- α, and IL-2.

3.6.3 Statistical Analysis

Quantitative colocalization data is presented as mean PCC +/- standard error of the mean. Sample sizes of n = 2 and n=6 were used for the initial and final *in vitro* experiments, respectively. The null hypothesis was that there is no difference in PCC between cells treated with chloroquine encapsulating particles and particles lacking chloroquine. A student's T-test was used to compare average PCC values at each timepoint, and a value of $p < 0.05$ was considered significant. A 2-way ANOVA was performed on data from the *in vivo* mouse experiments (n=3), with a Tukey post-hoc test. A value of $p < 0.05$ was considered significant.

4 Results

4.1 Nanoparticles

PLGA nanoparticles containing the following components were formulated successfully using either single or double emulsion solvent evaporation methods: R848, chloroquine, CD8 and SIINFEKL SLPs, SLPs conjugated to the VHL ligand, CD8 SLP conjugated to decane, and whole ovalbumin. Sizes determined by DLS were within the range of 191 and 561 nm (Table 1). Loading of peptides, chloroquine, and Resiquimod was determined with absorbance measurements. Particles were observed to maintain size throughout centrifugation and lyophilization processes, as measured by DLS (Fig. 13).

Table 1. Summary of PLGA nanoparticles that were formulated and characterized. Particles with a variety of components were fabricated using single and double emulsion methods. Loading of peptides, R848, and chloroquine was calculated using absorbance measurements, and DLS was used to determine particle sizes.

Components	Loading (ug / mg NP)	Chloroquine Loading (ug / mg NP)	Size (nm)	Emulsion Method
R848	23.3	--	561	o/w
CD8, Chlq	28.6	6.7	191	w/o/w
CD8-E3	17.5	--	369	o/w
CD8-E3 + Chlq	19.7	6.9	293	o/w
CD8-decyl + Chlq	72.96	22.43	206.9	w/o/w
SIINFEKL-E3	46.48	--	198.4	o/w
SIINFEKL-E3 + Chlq	22.94	3.3	228	o/w
CD8-E3-Cy5 + Chlq	1.66	9.05	243	w/o/w
SIINFEKL-E3-Cy5	3.11	--	231	w/o/w
OVA-E3	TBD	--	220.8	w/o/w

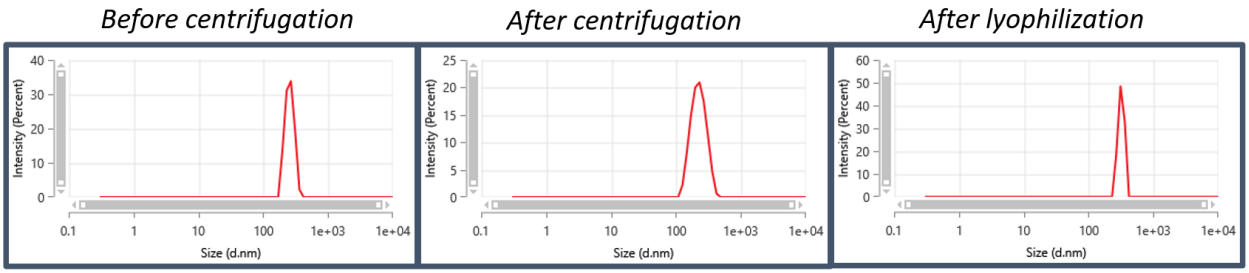

Figure 13. Representative DLS results prior to centrifugation, prior to lyophilization, and after lyophilization. Data depicted is from PLGA nanoparticles encapsulating CD8-E3 and chloroquine.

4.2 *In vitro* dose-response

Nanoparticles were formulated encapsulating Cy5-VHL-SLPs, one batch with chloroquine co-encapsulated and one without. The DC2.4 dendritic cells were treated for 4 h with a range of nanoparticle concentrations. Cells were fixed and covered with Immuno Mount DAPI and DABCO Mounting Media for nuclear staining. Several iterations of the dose-response experiment enabled the optimization of a functional experimental protocol, which was implemented in future *in vitro* studies such as the colocalization experiments.

Representative images were acquired for each dose at 63x magnification for Cy5 and DAPI channels. Doses between 0.05 and 0.1 mg NPs/mL (0.0125-0.025 mg/well) was deemed to be

appropriate to administer going forward. Qualitative comparative analysis of these images was possible, revealing that Cy5 fluorescence signal from the conditions with particles lacking chloroquine appeared to be more punctate than those which included chloroquine in the nanoparticle formulation (Fig. 14). This trend aligns with the rationale that nanoparticles without chloroquine would remain sequestered in endosomes, whereas chloroquine-encapsulating particles would promote endosomal escape and diffusion into the cytosol.

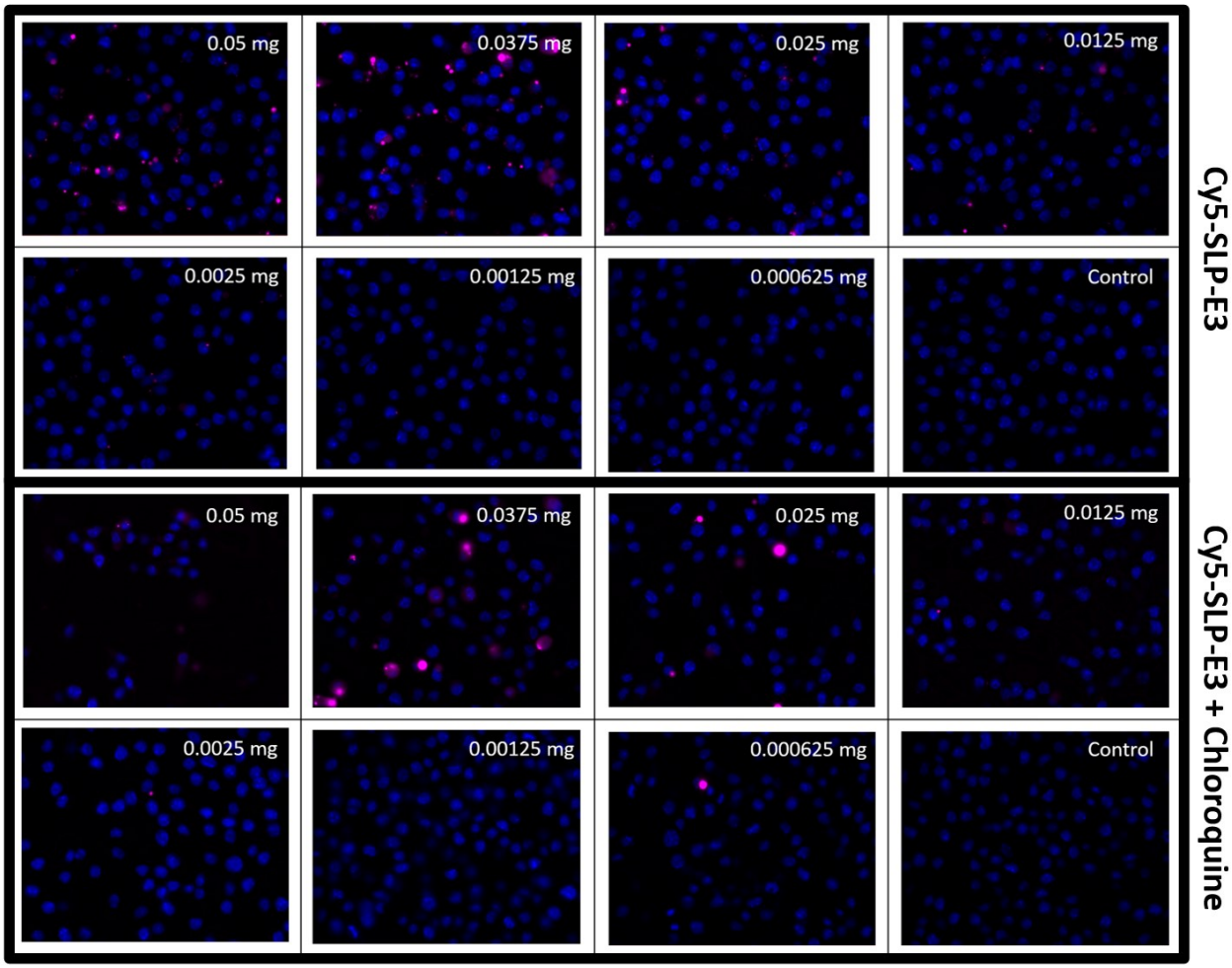

Figure 14. Fluorescent microscopy images acquired for the dose-response experiment. DAPI (nuclear stain) and Cy5 (fluorescent particles) channels are overlaid. A magnification of 63x was used. Uptake of particles by DC2.4s can be visualized by the Cy5 channel. Nanoparticles without chloroquine (top) and with chloroquine (bottom) were used to treat cells at a range of dosages (0.05, 0.0375, 0.025, 0.0125, 0.0025, 0.00125, 0.000625 mg particles per well).

4.3 Colocalization analysis over time

Dendritic cells were treated with nanoparticles with and without chloroquine for 4 h, then stained with Lysoview dye, fixed, and imaged over a range of timepoints (6 – 72 h) post-treatment. The objective of these experiments was to assess the cellular processing of the particles following endocytosis and determine whether co-encapsulation of chloroquine had a significant effect on endosomal escape. Upon initial uptake, PLGA particles are contained in early endosomes, which over the time course tested, acidify and transition into late endosomes and lysosomes, which are stained prior to fixation with the Lysoview dye. Images at 63x magnification were acquired upon completion of the experiments (Fig. 15). Cy5 and GFP image channels were inputted in the JaCoP colocalization plugin with Fiji software, and quantitative colocalization analysis was run on each replicate of each condition.

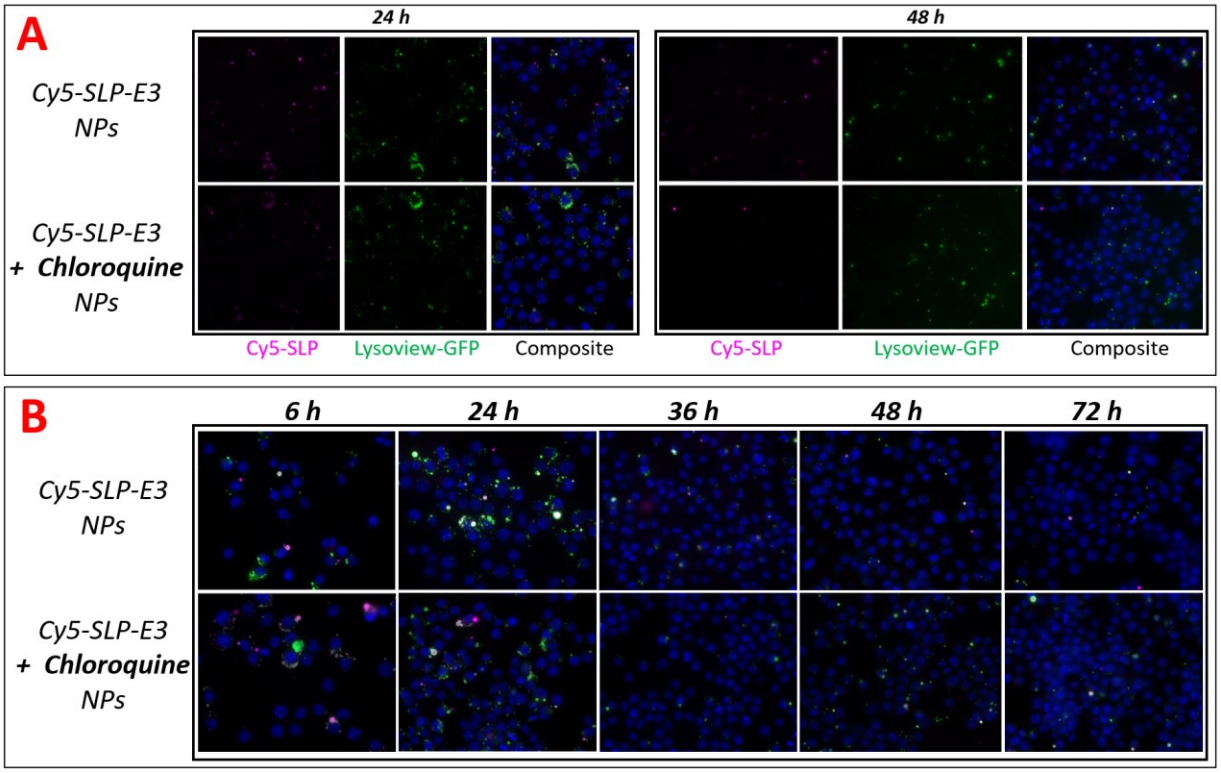

Figure 15. Representative images of dendritic cells dosed with particles containing Cy5-labeled SLP only and Cy5-labeled SLP with chloroquine. Pink corresponds to Cy5 fluorescent signal (labeled SLPs); green represents Lysoview-GFP dye staining lysosomes; blue corresponds to DAPI stain. Magnification of 63x with oil immersion was used to acquire all images. **A)** Cy5 and GFP channel images as well as a composite displaying Cy5, GFP, and DAPI channels overlaid for wells treated with +/- CQ particles at 24 h and 48 h. **B)** Representative composite images from 6, 24, 36, 48, and 72 h timepoints after treatment.

The first colocalization experiment showed promising results: over a period of 48 h, the Pearson correlation coefficient with the Costes method of thresholding between peptide (Cy5) and lysosome (GFP) channels remained relatively high (~0.7) when particles lacked chloroquine, but while the chloroquine positive conditions displayed similarly high PCCs at 6 h, the colocalization decreased with time post-treatment (Fig. 16). Experimental timepoints post-treatments included 6, 24, 36, 48 h. These results suggested that perhaps the co-encapsulated chloroquine was promoting SLP escape from endosomes and diffusion into the cytosol, whereas particles without chloroquine remained trapped within endosomal compartments as they reached the lysosomal stage. However, only 2 replicates per condition were tested in this initial experiment, and there was high variability within conditions.

Next, the colocalization experiment was repeated with n=6 over an extended time course (6, 24, 48, 72 h). Despite the expectation that decreased colocalization over time would be seen in chloroquine-positive particle conditions, as was seen in the preliminary experiment, PCC values were not significantly different between the two nanoparticle formulations, and the PCCs actually gradually increased over time. These results could indicate that the sensitivity of this colocalization analysis method is not sufficient for demonstrating advantages of chloroquine co-encapuslation for SLP endosomal escape.

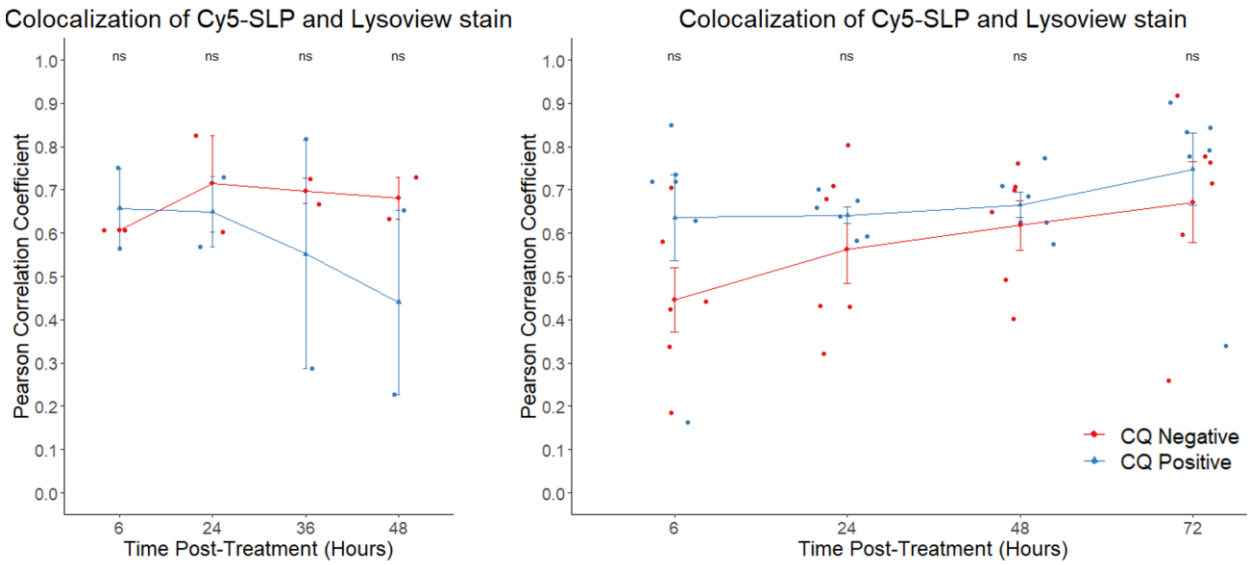

Figure 16. Pearson correlation coefficients (PCC) with Costes thresholding over time after treatment with nanoparticles with and without chloroquine encapsulation. Mean +/- standard error of the mean (SEM) PCC values are plotted for each experimental timepoint post-treatment. A student's t-test was performed to compare chloroquine-positive and -negative treatments at each timepoint. Blue corresponds to chloroquine-containing particle treatments; red represents the particle treatment conditions lacking chloroquine. Results from the earlier colocalization experiment over a 48 h time course are depicted on the left, n=2. Results from the final experiment with time points at 6, 24, 48, and 72 h are graphed on the right, n=6.

4.4 Engineered mRuby-Gal8 expressing DC2.4 and RAW264.7 cell lines

As an alternate strategy for quantification of endosomal escape efficiencies, development of cell lines expressing fluorescent Gal8 was explored. Due to application overlap with a different research project not discussed in this thesis, RAW264.7 murine macrophage cells were also engineered in parallel to the DC2.4 cells. Transfection of the mRuby-Gal8 plasmid was initially performed with a 4:1 mass ratio of transposon:transposase plasmids using a commercially available PEI transfection kit; however, this technique did not yield any cells positive for mRuby fluorescence as visually assessed using a fluorescent microscope. Next, transfection was attempted with a 6:1 ratio using a commercially available Lipofectamine LTX kit, following a RAW264.7 transfection protocol available online by Thermo Fisher [53]. Visual inspection using the red laser of the microscope demonstrated that both RAW264.7 and

DC2.4 cells were successfully transfected, albeit with relatively low transfection efficiency (~5%). Although a higher efficiency would be desirable, this was deemed sufficient, due to the accepted knowledge that DC2.4 and RAW264.7s are difficult-to-transfect cell lines. Cells were then cultured for a 7 d period, during which they were subcultured from the 48-well plates up to T25 culture flasks.

The transfected cells were next sorted for the mRuby-Gal8 positive populations via fluorescence activated cell sorting (FACS). The gating strategy that was applied is depicted in Figure 17. The first gate distinguished cells from non-cellular material by plotting SSC-Height vs. FSC-Height. Using those cells, the second gate was made by plotting SSC-Width vs. SSC-Height to select the single cell population. A DAPI stain was applied before sorting, which was used to partition live cells from dead cells. Lastly, a DAPI vs. mRuby fluorescent signal plot sorted the mRuby positive, single, live cells: this population was dispatched to the collection media for use in cell culture. Additionally, it was authenticated that the mRuby positive population was truly positive, and not due to autofluorescence, by looking at mRuby signal vs. signal from excitation by a 488 nm laser. mRuby has an excitation peak at 588 nm, and at 488 nm, excitation is only 9% of the maximum. Therefore, whereas autofluorescence would be indicated by a linear relationship between the two lasers, true mRuby signal is represented by a skewed trend where high mRuby signal does not correlate linearly with high signal from the 488 nm laser. This was indeed the finding during FACS of the transfected cells. Ultimately, 6×10^3 mRuby-Gal8+ RAW264.7 cells and 885 mRuby-Gal8+ DC2.4 cells were collected. One unfortunate factor that led to the low number of positive DC2.4s was the occurrence of a FACS instrument software malfunction during sorting; this necessitated sorting the cells twice, which resulted in fewer positive cells acquired and likely also influenced viability.

Due to the low number of sorted mRuby-Gal8+ cells, the cells were plated in single wells of a 24-well plate, rather than a T25 culture flask, in the anticipation that cell density would be sufficiently high for growth in the smaller surface area. After 2 d, the cells were examined on a fluorescence microscope;

images were acquired using the mRuby wavelength laser (Fig. 17). The cells post-sorting were visibly fluorescent. However, after 1 week in culture, with fresh growth medium replacements every 2 d, it was apparent that the cells were not proliferating adequately, and shortly thereafter cell detachment and death was observed.

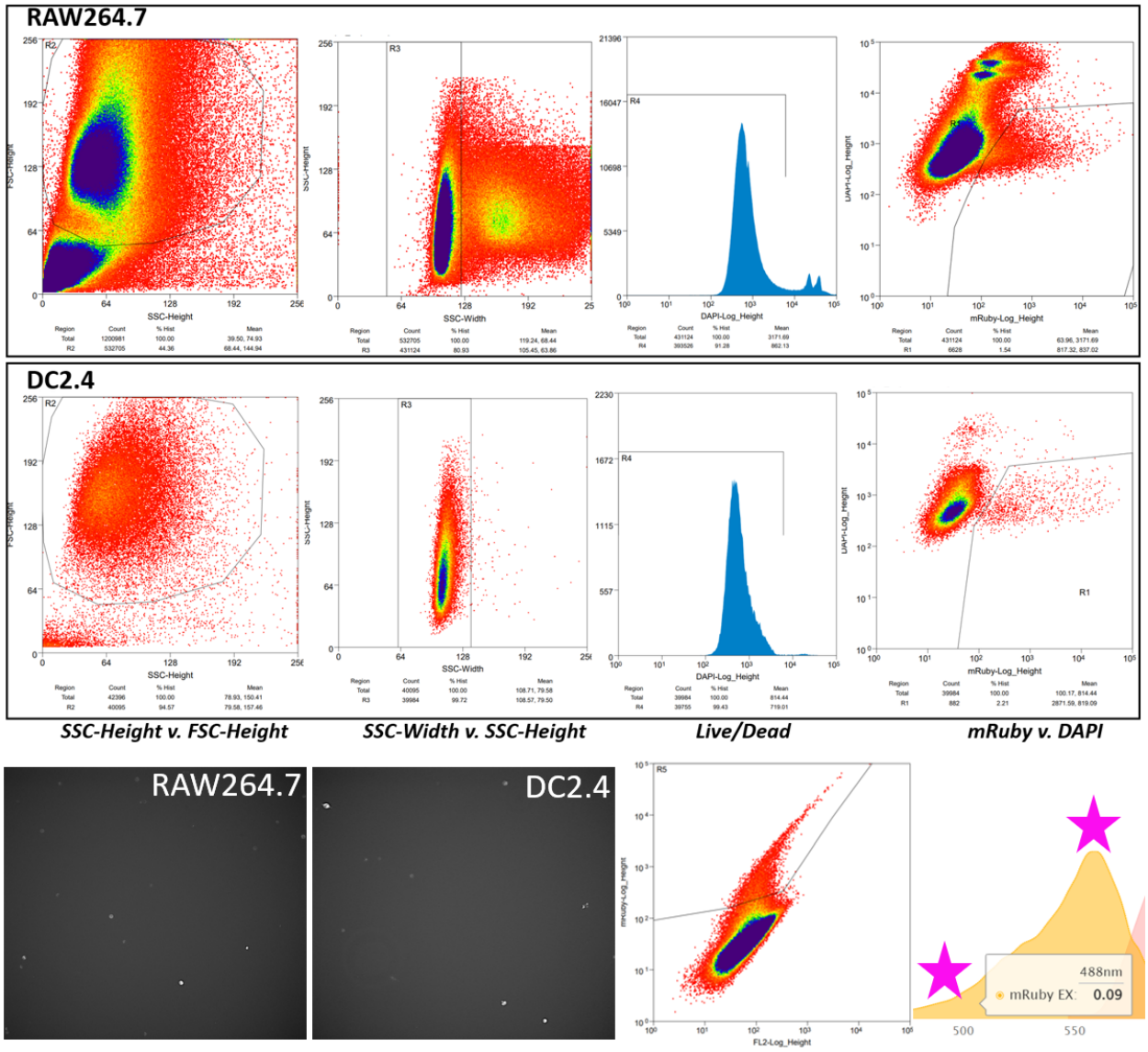

Figure 17. Gating strategy for fluorescent activated cell sorting of positive mRuby-Gal8 cells. Gating for cells, single cells, live cells, and finally mRuby+ cells was achieved using SSC-Height vs. FSC-Height, SSC-Width vs. SSC-Height, DAPI (live/dead), and mRuby vs. DAPI (live/dead), respectively. This FACS strategy was applied to both RAW264.7 and DC2.4 cells after transfection. Verification that mRuby+ signal was not ascribed to autofluorescence was confirmed by a skewed, non-linear relationship between mRuby signal and the 488 nm laser for which mRuby excitation is only 9% of its maximum. mRuby-Gal8 fluorescent cells were visually observed by microscopy 2 d after sorting and collection.

4.5 *In vivo* mouse vaccinations

At day 28 of the *in vivo* experiment, mice were sacrificed and cells were isolated from the spleen. The splenocytes were plated, then restimulated with antigen, thereby activating the antigen-specific T cells, which produce IFN-γ. The ELISPOT results depict the number of spots of IFN-γ-producing T cells per ten million cells upon antigen restimulation (Fig. 18). The highest relative number of IFN-γ-producing splenocytes was seen in the experimental group which received the full formulation of VHL-conjugated SLP and chloroquine co-encapsulated in nanoparticles, free CD4, and R848 encapsulated in particles. All groups that received the antigenic SLP had significant numbers of antigen-specific splenocytes, but statistical significance was only seen between the groups with VHL-conjugated SLP and chloroquine co-encapsulated in nanoparticles and the group with VHL-conjugated SLPs encapsulated in particles. This lack of differentiation between groups could be attributed to the fact that all groups received the same pDNA prime at day 0.

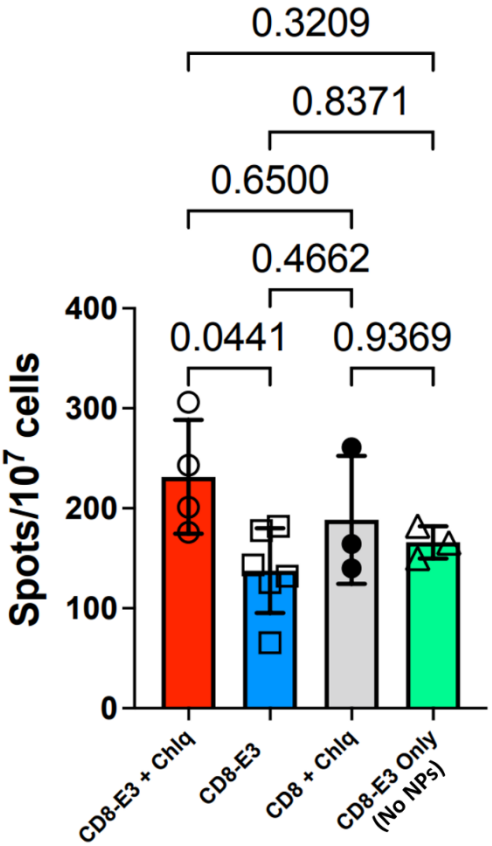

Figure 18. ELISPOT results from *in vivo* experiment. The relative number of IFN-γ-producing T cells (spots per 10 million cells) is plotted as mean +/- SEM for each experimental group. All groups depicted were administered free CD4-targeting SLPs and R848 encapsulated in PLGA particles. From left to right, groups were treated with PLGA NPs co-encapsulating VHL-SLPs + CQ, PLGA NPs encapsulating VHL-SLPs, PLGA NPs co-encapsulating unmodified SLPs + CQ, and free VHL-SLPs. For statistical analysis, a 2-way ANOVA was performed with a Tukey post-hoc test.

5 Discussion and future work

The next directions for this study fall into six main categories: 1) modified colocalization analysis methods for quantifying endosomal escape; 2) further nanoparticle characterization; 3) *in vivo* experiments vaccinating solely with nanoparticle formulations; 4) application of engineered mRuby-Gal8 cells in endosomal escape visualization and quantification; 5) testing of novel endosomal escape units; 6) demonstration of clinical disease relevance for HIV and other viral pathogens.

5.1 Endosomal escape quantification by colocalization

In the *in vivo* colocalization experiments performed thus far, no statistically significant difference was seen for PCC values between formulations containing and lacking the lysosomotropic agent chloroquine. These results were confounding, since it has been established previously that chloroquine is one of the most common promoters of endosomal escape [44]. Thus, there seem to be several possible explanations: the chloroquine dose delivered in the PLGA particles could be too low for efficacy; the sensitivity of the colocalization analysis method could be insufficient; the hydrolytic degradation of the PLGA particles could be too slow, obstructing the release of SLPs and chloroquine on the timescale of endosomal processes.

To address the potential that suboptimal chloroquine amounts were responsible for the unexpected outcome, the next step should be to formulate a new batch of PLGA nanoparticles that have chloroquine loading up to an order of magnitude higher than the 9.05 ug CQ / mg NPs tested so far. This could be accomplished by adding higher amounts of chloroquine during the oil-in-water emulsion. Alternatively, an amalgamation of Cy5-SLP-E3 + CQ particles and PLGA particles loaded only with chloroquine could be used for *in vitro* treatments, to maintain consistent peptide doses while raising the chloroquine dose. Regarding the colocalization method sensitivity, use of antibody staining rather than application of the Lysotracker dye could be useful for more precise monitoring of endosomal escape.

Antibodies against Rab5 (EEs), Rab7 (LEs), and LAMP-1 (lysosomes) can be purchased and used for the elucidation of endosomal mechanisms. If it the case that the PLGA nanoparticles do not undergo degradation by hydrolysis rapidly enough to facilitate the release of cargo, perhaps the polymeric particle confinement of chloroquine could reduce the weak base's ability to act as a proton buffer, or even if chloroquine is disrupting the endosome, enclosure of multimeric Cy5-SLPs within the particle could result in the prolonged punctate fluorescent signal seen. Since the 50:50 Poly(D,L-lactide-co-glycolide) ratio used in these formulations has the most rapid degradation kinetics of all PLGA compositions, lower molecular weight PLGA could be used, which corresponds to more rapid degradation [54].

5.2 Nanoparticle characterization

It will be sapient to continue refining and expounding upon methods for characterization of these nanoparticles. In this work, methods were established for determining particle sizes and using absorbance measurements to calculate loading of components within the particles. Ongoing HPLC quantification of peptide and chloroquine loading is underway. This involves generation of standard curves over a range of concentrations in which degraded nanoparticle component concentrations can be interpolated. Scanning electron microscopy (SEM) should also be performed for nanoparticle formulations to characterize particle size, shape, and morphology. Though no significant *in vitro* cytotoxicity was observed, an MTS toxicity assay should be performed to evaluate the impact of treatment with this subunit vaccine design on cell viability and proliferation.

5.3 Planned *in vivo* experiments

Another *in vivo* experiment with BALB/c mice has been planned, in which both the initial and boost injection will use the nanoparticle formulations, rather than a DNA prime, to better differentiate responses between groups. Additionally, this study will include a new experimental group which

receives the decyl-modified SLPs, serving as an inert VHL control. An *in vivo* experiment with VHL ligand-conjugated whole OVA proteins encapsulated in PLGA particles will be performed in the future. This will elucidate the potential capability of this PROTAC-based design to target whole proteins for proteasomal degradation and MHC I presentation to cytotoxic T lymphocytes. Conjugation of the NHS-functionalized PEG-VHL to OVA was successfully demonstrated in this study. Yet, full conjugation was not achieved even at a 30:1 NHS-PEG-VHL:OVA reaction ratio, meaning free OVA was still present. Ideally, all the OVA should be VHL-functionalized for particle formulations. It was hypothesized that the cause of incomplete conjugation was due to the quality of the precursor molecules used in the synthesis of NHS-PEG-VHL; new reactants have been ordered and will be used in conjugations going forward.

5.4 Gal8-fluorescent cells for endosomal disruption analysis

This research demonstrated the ability to develop mRuby-Gal8 DC2.4 and RAW264.7 cell lines using a 6:1 transposon:transposase ratio and a Lipofectamine LTX transfection kit. Since viability issues arose on account of the low quantity of mRuby-positive cells after FACS, transfection should be repeated in the same fashion, but then cells should be grown up to confluency in at least one T-75 cell culture flask to have a sufficient number of cells prior to FACS. The sterility of the sorter must be confirmed because activation of the dendritic cells or macrophages – for example, by lipopolysaccharides (LPS) – must be avoided.

Once cell lines stably expressing mRuby-Gal8 are established, these cells will be instrumental to *in vivo* investigation of endosomal disruption. The localization of Gal8 to endosomes upon rupture will provide direct visualization of endosomal escape processes. Live cell imaging and quantification is possible. Additionally, pulse shape analysis can be done with flow cytometric measurements: the width and height of the fluorescent pulse to evaluate endolysosomal escape [55]. In comparison to methods that use colocalization of fluorescent peptides and dyes to characterize endosomal escape, having a cell line that intrinsically reports events of endosomal disruption is particularly advantageous. Non-

fluorescently labeled peptides can be used, which not only mitigates spectral overlap but also provides versatility in the nanoparticle formulations used for *in vitro* analysis and a consistent, reproducible system for screening endosomal escape-promoting agents.

A future objective of this project is to incorporate novel endosomal escape units in the PROTAC-SLP vaccine formulation. Use of small-molecule chemical synthesis for creation of prodrug polymers will be explored. To this end, the optimized chloroquine system described in this work will be utilized as a baseline positive control for endosome-disruptive agents, against which novel units will be screened in the pursuit of finding superior candidates.

5.5 Demonstrate therapeutic advantages of this subunit vaccine

This subunit vaccine platform shows promise as a novel vaccination strategy to induce cell-mediated immunity. Ultimately, this aim of this research is to develop a therapeutically relevant subunit vaccine system capable of eliciting robust immunogenic CD8+ T cell responses that confers protective immunity against disease. In addition to demonstration of HIV-specific CD8+ T cell responses and presence of INF- γ, TNF- α, and IL-2, it is imperative that administration of this formulation results in effective HIV neutralization upon infection in the host. A shortcoming with traditional preclinical *in vivo* models is that the HIV virus cannot infect mice or rats. Humanized mouse models offer a solution to this limitation: these immunodeficient mice can be engrafted with human immune cells and are therefore able to acquire HIV infections. Numerous humanized mouse models have been employed in HIV research, with the bone marrow liver thymus (BLT) model accepted as the gold standard [57]. Testing this subunit vaccine design in humanized mice would be especially valuable, because it would provide a means to evaluate disease progression and survival outcomes after challenging the animals with an HIV infection.

Reaching beyond HIV vaccine applications, the PROTAC-SLP nanoparticle vaccine platform contrived in this research could demonstrate clinical applications for other infectious viral agents. The

system is amenable to substitution with virtually any synthetic azide-terminated SLP; therefore, any pathogenic infection to which the cytotoxic T cell response is fundamental could benefit from this technology.

6 References

[1] “HIV,” World Health Organization. [Online]. Available: https://www.who.int/news-room/fact-sheets/detail/hiv-aids. [Accessed: 08-Dec-2022].

[2] H. Du Rietz, H. Hedlund, S. Wilhelmson, P. Nordenfelt, and A. Wittrup, “Imaging small molecule-induced endosomal escape of Sirna,” Nature Communications, vol. 11, no. 1, 2020.

[3] M. Gros and S. Amigorena, “Regulation of antigen export to the cytosol during cross-presentation,” Frontiers in Immunology, vol. 10, 2019.

[4] M. Kovacsovics-Bankowski, K. Clark, B. Benacerraf, and K. L. Rock, “Efficient major histocompatibility complex class I presentation of exogenous antigen upon phagocytosis by macrophages.,” Proceedings of the National Academy of Sciences, vol. 90, no. 11, pp. 4942–4946, 1993.

[5] J. D. Colbert, F. M. Cruz, and K. L. Rock, “Cross-presentation of exogenous antigens on MHC I molecules,” Current Opinion in Immunology, vol. 64, pp. 1–8, 2020.

[6] G. Du and X. Sun, “Engineering nanoparticulate vaccines for enhancing antigen cross-presentation,” Current Opinion in Biotechnology, vol. 66, pp. 113–122, 2020.

[7] “Global statistics,” HIV.gov. [Online]. Available: https://www.hiv.gov/hiv-basics/overview/data-and-trends/global-statistics. [Accessed: 08-Dec-2022].

[8] S. Moir, T.-W. Chun, and A. S. Fauci, “Pathogenic mechanisms of HIV disease,” Annual Review of Pathology: Mechanisms of Disease, vol. 6, no. 1, pp. 223–248, 2011.

[9] A. Sáez-Cirión, M. Sinet, S. Y. Shin, A. Urrutia, P. Versmisse, C. Lacabaratz, F. Boufassa, V. Avettand-Fènoël, C. Rouzioux, J.-F. Delfraissy, F. Barré-Sinoussi, O. Lambotte, A. Venet, and G. Pancino, “Heterogeneity in HIV suppression by CD8 T cells from HIV controllers: Association with

GAG-specific CD8 T cell responses," The Journal of Immunology, vol. 182, no. 12, pp. 7828–7837, 2009.

[10]M. Angin, S. Volant, C. Passaes, C. Lecuroux, V. Monceaux, M.-A. Dillies, J. C. Valle-Casuso, G. Pancino, B. Vaslin, R. Le Grand, L. Weiss, C. Goujard, L. Meyer, F. Boufassa, M. Müller-Trutwin, O. Lambotte, and A. Sáez-Cirión, "Metabolic plasticity of HIV-specific CD8+ T cells is associated with enhanced antiviral potential and natural control of HIV-1 infection," Nature Metabolism, vol. 1, no. 7, pp. 704–716, 2019.

[11]"Immunity to HIV," Immunopaedia, 08-May-2018. [Online]. Available: https://www.immunopaedia.org.za/immunology/special-focus-area/5-immunity-to-hiv/. [Accessed: 08-Dec-2022].

[12]A. Galkin, Y. Chen, J. Guenaga, S. O'Dell, R. Acevedo, J. J. Steinhardt, Y. Wang, R. Wilson, C.-I. Chiang, N. Doria-Rose, A. V. Grishaev, J. R. Mascola, and Y. Li, "HIV-1 gp120–CD4-induced antibody complex elicits CD4 binding site–specific antibody response in mice," The Journal of Immunology, vol. 204, no. 6, pp. 1543–1561, 2020.

[13]A. B. McDermott and R. A. Koup, "Cd8+ T cells in preventing HIV infection and disease," AIDS, vol. 26, no. 10, pp. 1281–1292, 2012. Pfeifer, B. A., & Hill, A. (n.d.). Vaccine Delivery Technology Methods and Protocols Methods in Molecular Biology 2183. http://www.springer.com/series/7651

[14]L. Romanò, S. Paladini, C. Galli, G. Raimondo, T. Pollicino, and A. R. Zanetti, "Hepatitis B vaccination," Human Vaccines & Immunotherapeutics, vol. 11, no. 1, pp. 53–57, 2014.

[15]M. Pancera, A. Changela, and P. D. Kwong, "How HIV-1 entry mechanism and broadly neutralizing antibodies guide structure-based vaccine design," Current Opinion in HIV and AIDS, vol. 12, no. 3, pp. 229–240, 2017.

[16]R. J. Malonis, J. R. Lai, and O. Vergnolle, “Peptide-based vaccines: Current progress and future challenges,” Chemical Reviews, vol. 120, no. 6, pp. 3210–3229, 2019.

[17]M. Black, A. Trent, M. Tirrell, and C. Olive, “Advances in the design and delivery of peptide subunit vaccines with a focus on toll-like receptor agonists,” Expert Review of Vaccines, vol. 9, no. 2, pp. 157–173, 2010.

[18]P. Marrack, A. S. McKee, and M. W. Munks, “Towards an understanding of the adjuvant action of aluminium,” Nature Reviews Immunology, vol. 9, no. 4, pp. 287–293, 2009.

[19]A. S. Sameer and S. Nissar, “Toll-like receptors (tlrs): Structure, functions, signaling, and role of their polymorphisms in colorectal cancer susceptibility,” BioMed Research International, vol. 2021, pp. 1–14, 2021.

[20]J. Tel, S. P. Sittig, R. A. Blom, L. J. Cruz, G. Schreibelt, C. G. Figdor, and I. J. de Vries, “Targeting uptake receptors on human plasmacytoid dendritic cells triggers antigen cross-presentation and robust type I IFN secretion,” The Journal of Immunology, vol. 191, no. 10, pp. 5005–5012, 2013.

[21]D. Mahony, A. S. Cavallaro, F. Stahr, T. J. Mahony, S. Z. Qiao, and N. Mitter, “Mesoporous silica nanoparticles act as a self-adjuvant for ovalbumin model antigen in mice,” Small, vol. 9, no. 18, pp. 3138–3146, 2013.

[22]F. S. Tabatabaei Mirakabad, K. Nejati-Koshki, A. Akbarzadeh, M. R. Yamchi, M. Milani, N. Zarghami, V. Zeighamian, A. Rahimzadeh, S. Alimohammadi, Y. Hanifehpour, and S. W. Joo, “PLGA-based nanoparticles as Cancer Drug Delivery Systems,” Asian Pacific Journal of Cancer Prevention, vol. 15, no. 2, pp. 517–535, 2014.

[23]A. Bowen, E. E. Sweeney, and R. Fernandes, “Nanoparticle-based immunoengineered approaches for combating HIV,” Frontiers in Immunology, vol. 11, 2020.

[24]M. F. Bachmann and G. T. Jennings, “Vaccine delivery: A matter of size, geometry, kinetics and molecular patterns,” Nature Reviews Immunology, vol. 10, no. 11, pp. 787–796, 2010.

[25]B. Edagwa, J. E. McMillan, B. Sillman, and H. E. Gendelman, “Long-acting slow effective release antiretroviral therapy,” Expert Opinion on Drug Delivery, vol. 14, no. 11, pp. 1281–1291, 2017.

[26]H. H. Lara, N. V. Ayala-Nuñez, L. Ixtepan-Turrent, and C. Rodriguez-Padilla, “Mode of antiviral action of silver nanoparticles against HIV-1,” Journal of Nanobiotechnology, vol. 8, no. 1, p. 1, 2010.

[27]X. Wei, G. Zhang, D. Ran, N. Krishnan, R. H. Fang, W. Gao, S. A. Spector, and L. Zhang, “T-cell-mimicking nanoparticles can neutralize HIV infectivity,” Advanced Materials, vol. 30, no. 45, p. 1802233, 2018.

[28]R. Shahbazi, G. Sghia-Hughes, J. L. Reid, S. Kubek, K. G. Haworth, O. Humbert, H.-P. Kiem, and J. E. Adair, “Targeted homology-directed repair in blood stem and progenitor cells with CRISPR nanoformulations,” Nature Materials, vol. 18, no. 10, pp. 1124–1132, 2019.

[29]S. Mandal, M. Belshan, A. Holec, Y. Zhou, and C. J. Destache, “An enhanced emtricitabine-loaded long-acting nanoformulation for prevention or treatment of HIV infection,” Antimicrobial Agents and Chemotherapy, vol. 61, no. 1, 2017.

[30]C. J. Destache, S. Mandal, Z. Yuan, G. Kang, A. A. Date, W. Lu, A. Shibata, R. Pham, P. Bruck, M. Rezich, Y. Zhou, R. Vivekanandan, C. V. Fletcher, and Q. Li, “Topical tenofovir disoproxil fumarate nanoparticles prevent HIV-1 vaginal transmission in a humanized mouse model,” Antimicrobial Agents and Chemotherapy, vol. 60, no. 6, pp. 3633–3639, 2016.

[31]A. A. Murji, J. S. Qin, T. Hermanus, L. Morris, and I. S. Georgiev, “Elicitation of neutralizing antibody responses to HIV-1 immunization with nanoparticle vaccine platforms,” 2021.

[32]P. J. M. Brouwer and R. W. Sanders, “Presentation of HIV-1 envelope glycoprotein trimers on diverse nanoparticle platforms,” Current Opinion in HIV and AIDS, vol. 14, no. 4, pp. 302–308, 2019.

[33]F. Ferretti and M. Boffito, “Rilpivirine long-acting for the prevention and treatment of HIV infection,” Current Opinion in HIV and AIDS, vol. 13, no. 4, pp. 300–307, 2018.

[34]S. He, F. Gao, J. Ma, H. Ma, G. Dong, and C. Sheng, “Aptamer-PROTAC conjugates (apcs) for tumor-specific targeting in breast cancer,” Angewandte Chemie, vol. 133, no. 43, pp. 23487–23493, 2021.

[35]X. Li and Y. Song, “Proteolysis-targeting Chimera (PROTAC) for targeted protein degradation and cancer therapy,” Journal of Hematology & Oncology, vol. 13, no. 1, 2020.

[36]S.-L. Paiva and C. M. Crews, “Targeted protein degradation: Elements of PROTAC design,” Current Opinion in Chemical Biology, vol. 50, pp. 111–119, 2019.

[37]M. S. Gadd, A. Testa, X. Lucas, K.-H. Chan, W. Chen, D. J. Lamont, M. Zengerle, and A. Ciulli, “Structural basis of PROTAC cooperative recognition for selective protein degradation,” Nature Chemical Biology, vol. 13, no. 5, pp. 514–521, 2017.

[38]Maneiro María, N. Forte, M. M. Shchepinova, C. S. Kounde, V. Chudasama, J. R. Baker, and E. W. Tate, “Antibody–PROTAC conjugates enable HER2-dependent targeted protein degradation of BRD4,” ACS Chemical Biology, vol. 15, no. 6, pp. 1306–1312, 2020.

[39]C. Wang, C. Zheng, H. Wang, L. Zhang, Z. Liu, and P. Xu, “The state of the art of PROTAC Technologies for Drug Discovery,” European Journal of Medicinal Chemistry, vol. 235, p. 114290, 2022.

[40]J. Liu, H. Chen, L. Ma, Z. He, D. Wang, Y. Liu, Q. Lin, T. Zhang, N. Gray, H. Ü. Kaniskan, J. Jin, and W. Wei, “Light-induced control of protein destruction by opto-PROTAC,” Science Advances, vol. 6, no. 8, 2020.

[41]Y.-B. Hu, E. B. Dammer, R.-J. Ren, and G. Wang, “The endosomal-lysosomal system: From acidification and cargo sorting to neurodegeneration,” Translational Neurodegeneration, vol. 4, no. 1, 2015.

[42]N. Heath, X. Osteikoetxea, T. M. de Oliveria, E. Lázaro-Ibáñez, O. Shatnyeva, C. Schindler, N. Tigue, L. M. Mayr, N. Dekker, R. Overman, and R. Davies, “Endosomal escape enhancing compounds facilitate functional delivery of extracellular vesicle cargo,” Nanomedicine, vol. 14, no. 21, pp. 2799–2814, 2019.

[43]R. F. Minchin and S. Yang, “Endosomal disruptors in non-viral gene delivery,” Expert Opinion on Drug Delivery, vol. 7, no. 3, pp. 331–339, 2010.

[44]M. Agirre, J. Zarate, E. Ojeda, G. Puras, J. Desbrieres, and J. Pedraz, “Low molecular Weight Chitosan (lmwc)-based polyplexes for pdna delivery: From bench to bedside,” Polymers, vol. 6, no. 6, pp. 1727–1755, 2014.

[45]G. Yang, J. Zhang, W. You, X. Zhao, P. Hou, W. He, J. Yan, and H. Guo, “Targeted disruption of the bcl9/β-catenin interaction by endosomal-escapable nanoparticles functionalized with an e-cadherin-derived peptide,” Nanotechnology, vol. 31, no. 11, p. 115102, 2019.

[46]H. Sah, “A new strategy to determine the actual protein content of poly(lactide-co-glycolide) microspheres,” Journal of Pharmaceutical Sciences, vol. 86, no. 11, pp. 1315–1318, 1997.

[47]M. S. Cartiera, K. M. Johnson, V. Rajendran, M. J. Caplan, and W. M. Saltzman, “The uptake and intracellular fate of plga nanoparticles in epithelial cells,” Biomaterials, vol. 30, no. 14, pp. 2790–2798, 2009.

[48]K. W. Dunn, M. M. Kamocka, and J. H. McDonald, “A practical guide to evaluating colocalization in Biological Microscopy,” American Journal of Physiology-Cell Physiology, vol. 300, no. 4, 2011.

[49]S. V. Costes, D. Daelemans, E. H. Cho, Z. Dobbin, G. Pavlakis, and S. Lockett, “Automatic and quantitative measurement of protein-protein colocalization in live cells,” Biophysical Journal, vol. 86, no. 6, pp. 3993–4003, 2004.

[50]R. A. Day and E. M. Sletten, “Experimental perspectives on direct visualization of endosomal rupture,” ChemBioChem, vol. 22, no. 23, pp. 3277–3282, 2021.

[51]K. V. Kilchrist, S. C. Dimobi, M. A. Jackson, B. C. Evans, T. A. Werfel, E. A. Dailing, S. K. Bedingfield, I. B. Kelly, and C. L. Duvall, “GAL8 visualization of endosome disruption predicts carrier-mediated biologic drug intracellular bioavailability,” ACS Nano, 2019.

[52]*“Transfecting plasmid DNA into RAW264.7 macrophage cells using lipofectamine LTX reagent,” Thermo Fisher Scientific - US. [Online]. Available: https://www.thermofisher.com/us/en/home/references/protocols/cell-culture/transfection-protocol/transfecting-plasmid-dna-into-raw267-3-macrophage-cells-using-lipofectamine-ltx-reagent.html#:~:text=Lipofectamine%C2%AE%20LTX%20Reagent%20is,Lipofectamine%C2%AE%20LTX%20Reagent%20(Cat. [Accessed: 08-Dec-2022].*

[53]M. Tracy, “Factors affecting the degradation rate of poly(lactide-co-glycolide) microspheres in vivo and in vitro,” Biomaterials, vol. 20, no. 11, pp. 1057–1062, 1999.

[54]H. J. Wensley, D. A. Johnston, W. S. Smith, S. E. Holmes, S. U. Flavell, and D. J. Flavell, “A flow cytometric method to quantify the endosomal escape of a protein toxin to the cytosol of target cells,” Pharmaceutical Research, vol. 37, no. 1, 2019.

[55]A. Gillgrass, J. M. Wessels, J. X. Yang, and C. Kaushic, “Advances in humanized mouse models to improve understanding of HIV-1 pathogenesis and immune responses,” Frontiers in Immunology, vol. 11, 2021.